NASA Contractor Report 3190

Gas Phase Hydrogen Permeation in Alpha Titanium and Carbon Steels

Donald L. Johnson, Kiritkumar K. Shah,
Bruce H. Reeves, and Vijay L. Gadgeel

GRANT NGR 28-004-025
APRIL 1980

NASA

NASA Contractor Report 3190

Gas Phase Hydrogen Permeation in Alpha Titanium and Carbon Steels

Donald L. Johnson, Kiritkumar K. Shah,
Bruce H. Reeves, and Vijay L. Gadgeel
University of Nebraska
Lincoln, Nebraska

Prepared for
Ames Research Center
under Grant NGR 28-004-025

National Aeronautics
and Space Administration

**Scientific and Technical
Information Office**

1980

SYMBOLS

a	interior radius of a hollow, cylindrical membrane (cm)
b	exterior radius of a hollow, cylindrical membrane (cm)
C	subsurface equilibrium hydrogen concentration (cm^3(NTP) cm^{-3})
C_{g_a}, C_{g_b}	hydrogen gas concentration at the interior and exterior of a hollow cylindrical membrane
C_s	hydrogen adatom concentration
D	coefficient of hydrogen diffusion within the metal lattice (cm^2 s^{-1})
D_o	pre-exponential constant for hydrogen diffusion
ΔH_s	heat of solution (j $mole^{-1}$)
h_a	reaction rate constant at a
h_b	reaction constant at b
I	RGA output current
j_T	theoretically derived permeation or hydrogen flow rate through a hollow cylindrical membrane (cm^3 s^{-1})
K_s	partition constant
K'	Sievert's constant
K_g	ratio of hydrogen gas concentration to hydrogen adatom concentration
n	pressure dependence
p_a	hydrogen partial pressure at a
p	empirically derived permeation or hydrogen flow rate through a hollow cylindrical membrane (mole s^{-1} or molecules s^{-1})
p_o	permeation pre-exponential constant
p'_o	permeation pre-exponential constant corrected for pressure
Q_D	activation energy for hydrogen diffusion (j $mole^{-1}$)
Q_p	activation energy for hydrogen permeation (j $mole^{-1}$)
s	time (seconds)

T	absolute temperature of a hollow cylindrical membrane (°K)
t_L	lag-time parameter for nonsteady state transport (s)
θ, v	calibration constants
ϕ	coefficient for hydrogen permeation under steady state conditions through the metal lattice (cm^3 (NTP) cm^{-1} s^{-1} $(Nm^{-2})^{-\frac{1}{2}}$)
ϕ_o	pre-exponential constant for coefficient of hydrogen permeation
α_a	geometric parameter for interior surface reaction control (cm^{-2})
α_b	geometric parameter for exterior surface reaction control (cm^{-2})
α_D	geometric parameter for diffusion control (cm^{-2})

PART I

GAS-PHASE HYDROGEN PERMEATION AND DIFFUSION IN ALPHA TITANIUM FROM 400-800°C

Donald L. Johnson, Kiritkumar K. Shah and Bruce H. Reeves

University of Nebraska

SUMMARY

Commercially pure titanium rods were machined into hollow cylinders and gas-phase permeation and diffusion measurements obtained with a quadrupole residual gas analyzer at temperatures between 400-800°C and pressures between 0.533 and 266.6 Nm^{-2}. Pressure dependence measurements established that phase boundary reactions as well as lattice diffusion control the transport process. Lag-time data yield excellent agreement with the diffusivity data of Wasilewski and Kehl and Papazoglou and Hepworth for the case where phase boundary reactions are taken into account. The best value of the diffusivity is $D = 2.1 \times 10^{-2} \exp(-50{,}400/RT)$. Analysis of lag-time data reveals that unsteady state transport tends toward phase boundary reaction control for thin membranes (low b/a ratio) and diffusion control for thick membranes (large b/a ratio). Permeation activation energy, Q_p, is 74,300 Joules $mole^{-1}$. Due to first power pressure dependency, P_o values are a complex function of pressure and geometry and are presented in tabular form. Oxide and nitride films on the interior membrane surface retard permeation whereas the same films on the exterior surface enhance the permeation somewhat. This is explained in terms of a discontinuous TiH_2 layer.

INTRODUCTION

In recent years there has been increasing interest in developing a quantitative understanding of the process of hydrogen transport in titanium and titanium alloys (refs. 1,2,3). This interest has developed because of their use in high temperature applications in the aerospace industry. Titanium alloys are frequently used in environments where embrittlement or corrosion by hydrogen can occur. It is well known that a very small amount of hydrogen, on the order of 90-150 parts per million (less than 1 atomic percent), causes embrittlement and loss of ductility but has little effect on tensile properties at room temperature (ref. 4).

Titanium is capable of absorbing hydrogen from a number of sources, including ammonia, water vapor, propane, and other hydrocarbons when heated in their presence. This is a hydrogen environment embrittlement phenomenon in which embrittlement of titanium under stress results from presence of gaseous hydrogen. Williams (ref. 5) has described the subject of hydrogen

contamination and also reaction kinetics and methods for reducing or eliminating hydrogen contamination.

It has been suggested (ref. 6) that the observed brittleness of titanium exposed to hydrogen environments is due to the presence of microcracks, pores, and fissures caused by 17.2% volume expansion when hexagonal alpha titanium reacts with hydrogen to form titanium hydride (TiH_2). Other studies (refs. 7, 8) confirmed the importance of hydriding and dehydriding kinetics.

Wasilewski and Kehl (ref. 10) and Papazoglou and Hepworth (ref. 11) have determined the diffusivity of hydrogen in α-Ti as a function of temperature at various pressures. The technique used in both instances involved the admission of hydrogen gas to a reaction vessel of known volume and the monitoring of absorbed volume as a function of time. They determined diffusivities by correlating this time dependent flux with the time dependent solution to Fick's second law. Wasilewski and Kehl's data are given by $D_{(\alpha)} = 1.8 \times 10^{-2} \exp(-51{,}800 \pm 2845)/RT$ and Papazoglou and Hepworth's by $D_{(\alpha)} = 3.0 \times 10^{-2} \exp(-61{,}500 \pm 2720)/RT$. The difference in the two sets of data probably reflects the way in which the experiments were conducted. Wasilewski and Kehl took advantage of the β-phase stabilizing effect of hydrogen to form a β-Ti surface layer on the α-Ti membrane. This surface layer, saturated with hydrogen, then acted as a constant hydrogen source to the interior α-phase. Papazoglou and Hepworth introduced hydrogen into the α-phase directly from the gas phase at low enough pressures to prevent the formation of β-phase. Temperature and pressure limits in the later case were determined from solubility data (refs. 12,13). Prior to the present work, there was no systematic study of the influence of pressure and temperature on the hydrogen permeation through α-Ti. However, there have been several attempts to determine hydrogen permeation rates through container walls (ref. 14) under specific conditions.

There are several reports on the reaction between titanium and hydrogen and the effect of oxygen or oxide film on it. Wickstrom and Etheridge (ref. 15) thought that scratching, abrading or thermal and pressure cycling of titanium components exposed the reactive titanium surface to hydrogen and promoted the formation of extremely brittle titanium hydride. Gilb and Kruschwitz (ref. 6) reported that traces of oxygen and possibly other gases as impurities in hydrogen markedly retarded its reaction rate with titanium. Recently, Caskey (ref. 16) studied in detail the influence of a surface oxide film on hydriding of titanium and found that the oxide film retards the formation and precipitation of hydride. Reichardt (ref. 17) mentioned the inhibiting effect of titanium surface contamination on the reaction of hydrogen with the metal and a similar explanation was employed by Wasilewski and Kehl (ref. 10) to explain the low initial reaction rates observed. They also found that the rate was sensitive to the surface oxide film, and that the continuance of the low reaction rates was a function of the degree of surface oxidation. Schoenfelder and Swisher (ref. 8) attributed the reduction in the rate of decomposition of titanium hydride to the diffusion of hydrogen through the surface oxide film. Williams and Maykuth (ref. 18) concluded that a rapid reaction of hydrogen with titanium at ambient temperature is promoted by a clean metal surface. They interpreted the failure to observe the reaction at

ambient temperature as due to the presence of surface oxides on the metal and to impurities in the hydrogen.

From the preliminary studies (ref. 9) conducted at Nebraska, nitride surface film seems to have an effect on the rate of permeation similar to that of an oxide film. However, the nitride film thickness necessary to reduce the rate of permeation was estimated to be an order of magnitude less. No other work is reported on the effect of surface nitride films on hydrogen permeation through alpha titanium.

The primary objectives of Part I of this project were to 1) determine the kinetic rate parameters for gas-phase hydrogen permeation and diffusion in alpha titanium, 2) establish the location of the reactions which control the rate of permeation, and 3) determine the effect of oxide and nitride films on the permeation rate. The two techniques used in reaching these objectives were nonsteady state lag-time measurements and steady state permeation. The four variables examined were membrane geometry, temperature, hydrogen partial pressure and surface treatment.

THEORETICAL CONSIDERATIONS

Permeation

A generalized expression (ref. 1) for the permeation rate is given by

$$j_T = \frac{2\pi \ell K_s \left(C_{g_a} - C_{g_b}\right)}{K_s/ah_a + K_s/bh_b + \ell n(b/a)/D} \tag{1}$$

where the first two terms in the denominator characterize transport resistance at inlet and outlet surfaces and the third term in the denominator characterizes transport through the lattice of the bulk metal. Since $K_s (C_{g_a} - C_{g_b})$ is directly proportional to the square root of the partial pressure according to Sievert's law, $K_s C_{g_a} = K' K_g P_a^{\frac{1}{2}}$ (refs. 1,2); and equation (1) has the alternate general form where $C_{g_b} \cong 0$:

$$j_T = \frac{2\pi \ell K' K_g \left(p_a^{\frac{1}{2}}\right)}{K_s/ah_a + K_s/bh_b + \ell n(b/a)/D} \tag{2}$$

Examination of equation (2) reveals that there is no simple way to describe permeation as a function of geometry for the completely general case where surface reactions as well as diffusion are involved in the transport process. However, for the case where lattice diffusion is controlling and $h_a = h_b >> D$, the two surface terms disappear to give

$$j_T = \frac{2\pi \ell D K' K_g p_a^{1/2}}{\ell n(b/a)} \tag{3}$$

A plot of j_T versus $[\ell n(b/a)]^{-1}$ from equation (3) is linear at constant temperature and pressure and is a means to test its validity. If such a plot is nonlinear, equation (2) is applicable since both lattice diffusion and surface reactions are operative in the transport process. The validity of equation (3) can also be determined from pressure dependent measurements at constant temperature and specimen radii. Equation (3) reduces to equation (4)

$$j_T = (\text{Constant})\ p_a^{1/2} \tag{4}$$

$$\ell n(j_T) = 1/2\ \ell n(p_a) + (\text{Constant})' \tag{5a}$$

or in general

$$\ell n(j_T) = n\ \ell n(p_a) + (\text{Constant})' \tag{5b}$$

A log-log plot of j_T versus p_a is linear with slope 1/2 if diffusion controls the transport. If the slope is between 1/2 to 1, transport is partially or totally controlled by surface reactions.

Two cases are of special interest:

Case I - Combined Surface and Lattice Diffusion Control

There is no practical theoretical model to describe permeation as a function of pressure and geometry. For a given geometry, an empirical temperature dependent expression for permeation is given by

$$P = P_o \exp(-Q_p/RT) \tag{6a}$$

Pressure dependence may be included in equation (6a) by setting

$$P_o = P_o' p_a \quad \text{(ref. 3)} \tag{6b}$$

Case II - Lattice Diffusion Control

Equation (3) is converted to equation (7) by combining constants and inserting the coefficient of permeation as follows:

$$j_T = \phi \frac{2\pi \ell}{[\ell n(b/a)]} p_a^{1/2} \tag{7}$$

Temperature dependence is introduced into the coefficient of permeation by

$$\phi = \phi_o \exp(-Q_p/RT) \tag{8}$$

Diffusion

Derivation of a generalized expression for lag time in the gas-phase permeation of hollow cylinders has been discussed elsewhere (refs. 19,20). The generalized equation may be simplified to three cases of practical interest:

1) Surface reactions are very rapid compared with bulk diffusion, h_a and $h_b >> sD$

$$\alpha_D = 1/Dt_L \tag{9}$$

where $$\alpha_D = 4\ell n\,(b/a) / [(b^2 + a^2)\,\ell n\,(b/a) - (b^2 - a^2)] \tag{10}$$

2) Reactions occurring at the outlet surface are infinitely rapid and bulk diffusion as a result of a concentration gradient is very rapid compared with reactions occurring at the inlet surface, $h_b \to \infty$, $h_a << sD$

$$\alpha_a = 1/Dt_L \tag{11}$$

where $$\alpha_a = 4 / [b^2 - a^2 - 2a^2\,\ell n\,(b/a)] \tag{12}$$

3) Surface reactions occurring at the inlet surface are infinitely rapid and bulk diffusion as a result of concentration gradient is very rapid compared with reactions occurring at the outlet surface, $h_a \to \infty$, $h_b << sD$

$$\alpha_b = 1/Dt_L \tag{13}$$

where $$\alpha_b = 4 / [2b^2\,\ell n\,(b/a) - (b^2 - a^2)] \tag{14}$$

It can be seen from the above equations that diffusivity and lag time are functionally dependent upon inlet and outlet specimen radii. The lag time can be expressed in the form of an Arrhenius equation

$$1/t_L = (1/t_L)_o \exp(-Q_D/RT) \tag{15}$$

Substituting equations (9) and (10), (11) and (12) or (13) and (14) into (15) gives

$$D = D_o \exp(-Q_D/RT) \tag{16}$$

Q_D may be compared with the results of others (refs. 10,11) where a plot of $\ell n(D)$ versus $1/T$ is linear with a slope of $-Q/R$ and intercept D_o. The pre-exponential constant, D_o, determines the validity of the three equations (9), (11) and (13). By comparing results to those obtained by others for α-titanium, it is possible to determine for each geometry whether diffusion, interior surface reactions, or exterior surface reactions or some combination of the three controls the overall rate of hydrogen transport. Furthermore, a plot of $1/t$ versus $1/\alpha$ depicts the variation of experimental points with geometry about some line based on a known value of the diffusion coefficient at constant temperature. For diffusion control, D is constant for all α_D (geometric configuration parameter) according to equation (10) so that

$$1/t_L \cdot 1/\alpha_D = D \tag{17}$$

Taking the logarithm of each side:

$$\ell n(1/t_L) = \ell n(D) - \ell n\,(1/\alpha_D) \tag{18a}$$

Similarly, for interior surface reaction control and exterior surface reaction control respectively:

$$\ell n(1/t_L) = \ell n(D) - \ell n\,(1/\alpha_a) \tag{18b}$$

$$\ell n(1/t_L) = \ell n(D) - \ell n\,(1/\alpha_b) \tag{18c}$$

A plot of $\ell n(1/t_L)$ versus $\ell n(1/\alpha)$ for each of the three cases is a straight line of slope -1. Since D is known (refs. 10,11), a reference line may be drawn to establish which of the three cases gives the best correlation of the data.

Solubility

For lattice diffusion controlled transport, gas phase hydrogen is in thermodynamic equilibrium with subsurface hydrogen and the solubility is given by the ratio of permeability to diffusivity. In terms of the coefficients of permeation and diffusion, the relationship is given by

$$C = \frac{\phi}{D} p_a^{\frac{1}{2}} \tag{19}$$

Since for partial or complete surface reaction control, gas phase hydrogen is not in equilibrium with subsurface hydrogen, the solubility cannot be calculated from transport data.

TEST MATERIALS

Chemical Analysis

A total of twenty specimens were prepared for examination from commercially pure titanium rod obtained through Astro-metallurgical and G. O. Carson, Inc. Typical analysis from the former were 0.005 - 0.015 w/o C, .06 - .14 w/o Fe, .082 w/o O, .009 - .015 w/o N, .0009 - .0059 w/o H and balance Ti. Analysis from the latter were .07 w/o C, .13 w/o Fe, 0.24 w/o O, .02 w/o N, 0.0047 w/o H and balance Ti.

Specimen Geometries

The geometries of "S" series specimens were chosen more or less randomly and were numbered from 1S1 through 4S5 as listed in Table I. The geometries of A-B series specimens were chosen to establish two series of variables, those with a constant interior radius and varying exterior radii and those with a constant exterior radius and varying interior radii. Specimens designated "B" indicate those with a constant exterior radius (b=0.489 cm) and similarly, those designated with an "A" correspond to specimens with a constant interior radius (a=0.320 cm). The exterior radii were chosen such that each set, A and B had the same radius ratio. All specimen lengths were 7.5 inches (19.05 cm). The geometry data given in Table I applies to a 2.54 cm gage length as shown in Figure 1.

TABLE I. - SPECIMEN GEOMETRY DATA

Specimen	Exterior radius b (cm)	Interior radius a (cm)	Wall thickness (b-a) (cm)	(b/a)	$[\ell n(b/a)]^{-1}$
1AS2	0.4890	0.4369	0.0521	1.119	8.916
3S2	0.5410	0.4902	0.0508	1.103	10.12
4S2	0.4356	0.3571	0.0785	1.220	5.026
1S3	0.5156	0.4369	0.0787	1.180	6.039
2S4	0.5004	0.4369	0.0635	1.145	7.386
3S4	0.6185	0.3200	0.2985	1.933	1.517
7S5	0.4890	0.2540	0.2350	1.925	1.527
4S5	0.4890	0.4242	0.0648	1.153	7.026
1-A	0.513	0.320	0.193	1.603	2.12
1-B	0.489	0.305	0.184	1.603	2.12
2-A	0.405	0.320	0.085	1.266	4.24

(continued)

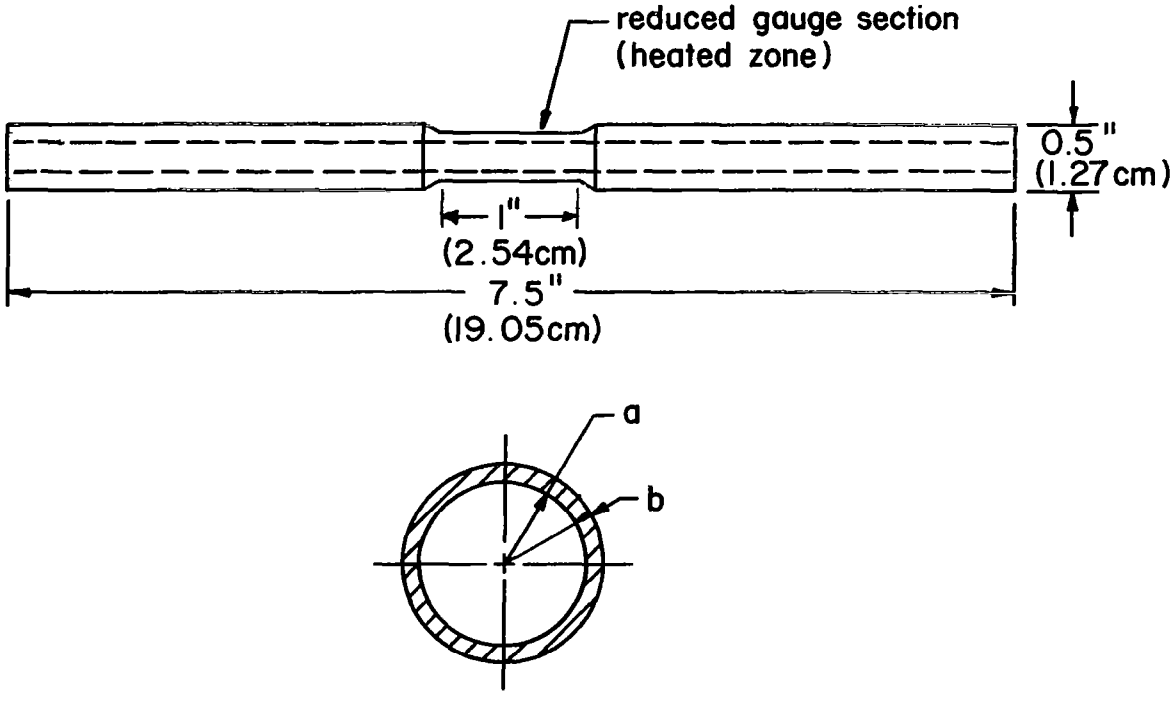

Figure 1. - Geometric configuration of hollow cylindrical membranes

TABLE I. - continued

Specimen	Exterior radius b (cm)	Interior radius a (cm)	Wall thickness (b-a) (cm)	(b/a)	$[\ln(b/a)]^{-1}$
2-B	0.489	0.386	0.103	1.266	4.24
4-A	0.370	0.320	0.050	1.155	6.94
9-A	0.450	0.320	0.130	1.405	2.94
9-B	0.489	0.348	0.141	1.405	2.94
11-A	0.560	0.320	0.240	1.750	1.79
11-B	0.489	0.279	0.215	1.753	1.79

EXPERIMENTAL

Test System

The experimental system and components, presented in Figure 2, is similar to that developed by Frauenfelder (ref. 21) and others (refs. 3,39). The most important aspect of the system is that it utilizes highly sensitive mass spectrometry to measure hydrogen flow rate.

The test system consists of two ultrahigh vacuum systems, an input system used for the introduction of hydrogen into the specimen and an output system for the analysis and removal of the permeated hydrogen.

Specimens were machined to gage section, polished through 600 grit paper and ultrasonically cleaned in acetone before mounting in the test system. The A-B series titanium specimens were chemically polished in an acid solution of 75 ml HNO_3, 15 ml HF and 15 ml H_2SO_4. The entire system was helium leak checked and subsequently pumped to the 10^{-9} torr range. The specimen was then slowly heated to test temperature while the ion-pump continued to remove outgassed hydrogen and other residual gases. A steady-state background was achieved prior to each test run.

Steady-state permeation measurements were obtained by valving out the ion-pump on the input system and backfilling with nitrogen cold-trapped hydrogen to the desired pressure as determined on the alphatron pressure gage for pressures up to about 1.866×10^5 Nm^{-2} (1400 torr). Above this pressure, a conventional diaphram type gage was used. Constant pressure was maintained by manual control of the leak valve. The mass spectrometer (residual gas analyzer) in the output system simultaneously monitored the hydrogen permeating the cylindrical wall of the specimen until the permeating flux became constant. Specimen temperature was controlled manually to about ± 3°C.

Nonsteady state lag time measurements (refs. 22,23) were made to determine the diffusion coefficient. Hydrogen was introduced to a precalibrated reservoir,

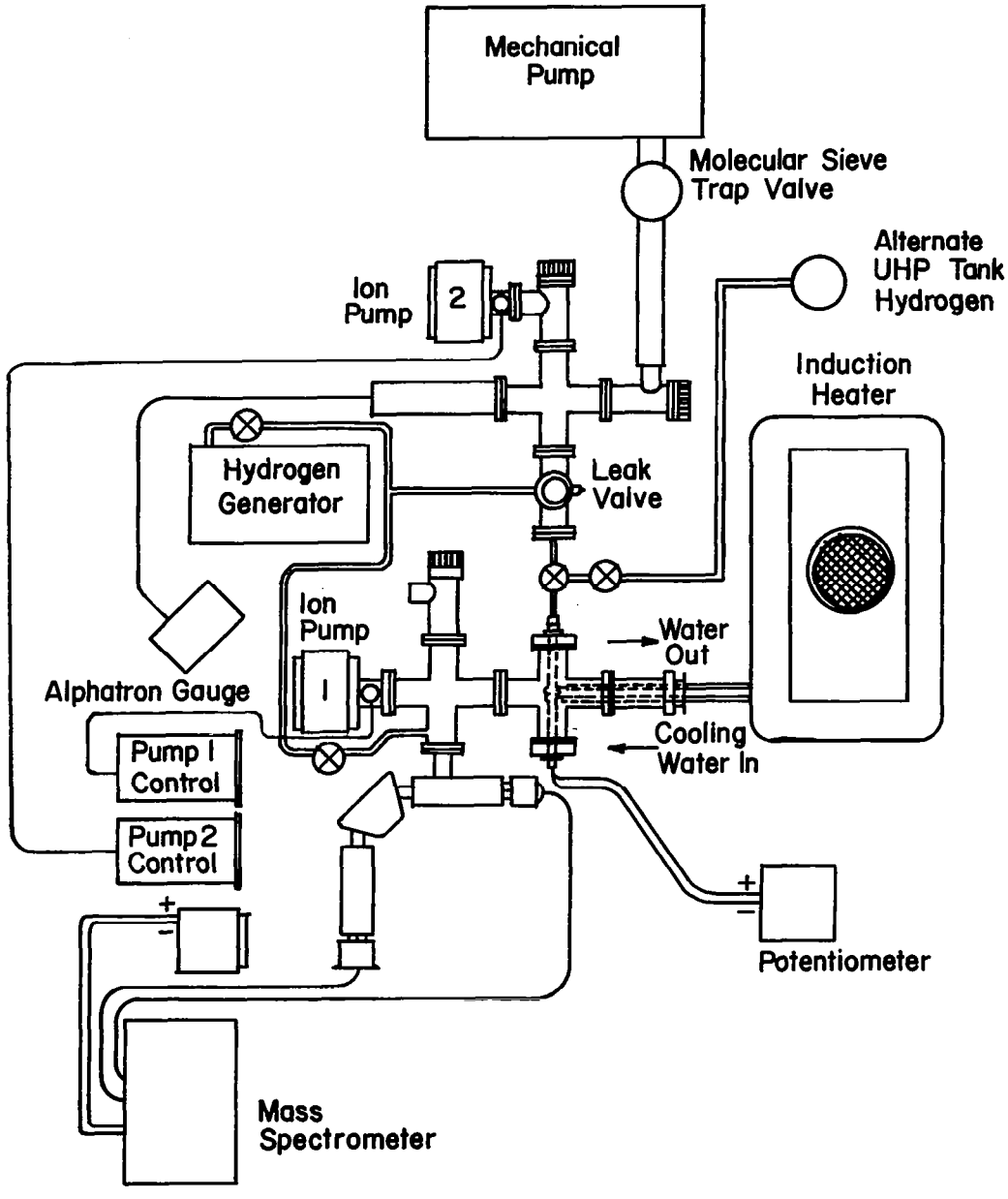

Figure 2. - Experimental system

an isolation valve was opened, and contact was made with the specimen at a predetermined pressure. Simultaneous with hydrogen contact, the mass spectrometer began recording the hydrogen flux. Due to the low hydrogen input pressure required to prevent formation of β-phase in Ti, the mass spectrometer output had to be maintained near maximum sensitivity to obtain a well defined current profile. In order to obtain a single profile of time vs. flux, the data were replotted on graph paper and the linear portion of the curve was extrapolated to zero flux. The intercept at zero flux is the delay time, t_L.

Calibration

Calibration for hydrogen flow through the mass spectrometer was achieved by a standard known conductance technique (ref. 24). According to Figure 3, the measured calibration factor is 1.68 X 10^{26} molecules s^{-1} amp^{-1} for the G.E. model 514 RGA. This unit was used for all titanium experiments. A new Varian quadrupole RGA was used on subsequent experiments involving iron and carbon steels. In the latter case, a plot similar to Figure 3 gave a calibration factor of 1.425 X 10^{24} molecule s^{-1} amp^{-1}.

RESULTS

Permeation

The permeation parameters P_o and Q_p defined by equation (6a) are presented in Table II for both the S series and the A-B series specimens. Additional data are presented in Table III at 600°C. The variables represented by the data in the tables are incorporated into graphical illustrations in the following sections.

TABLE II. - HYDROGEN PERMEATION PARAMETERS IN ALPHA TITANIUM AS A FUNCTION OF TEMPERATURE, PRESSURE AND SPECIMEN GEOMETRY

Specimen	T (°C)	p_a (Nm^{-2})	$[\ell n(b/a)]^{-1}$	P_o X 10^{-20} (molecules s^{-1})	Q_p (J $mole^{-1}$)
3S2	732-798	2.67 (.02 torr)	10.12	0.298	71,130 ± 2700
	721-801	5.33 (.04 torr)		0.540	
4S2	636-750	2.67	5.03	0.182	72,380
	571-720	5.33		0.364	72,380
	423-653	26.66 (.2 torr)		1.82	72,380
1AS2	541-648	5.33	8.92	1.75	69,290
7S5	605-661	5.33	1.53	2.68	76,340
1S3	540-767	5.33	6.04	0.57	71,060
	463-750	26.66		2.80	71,060
1A	600-645	5.33	2.12	1.47	75,670

continued

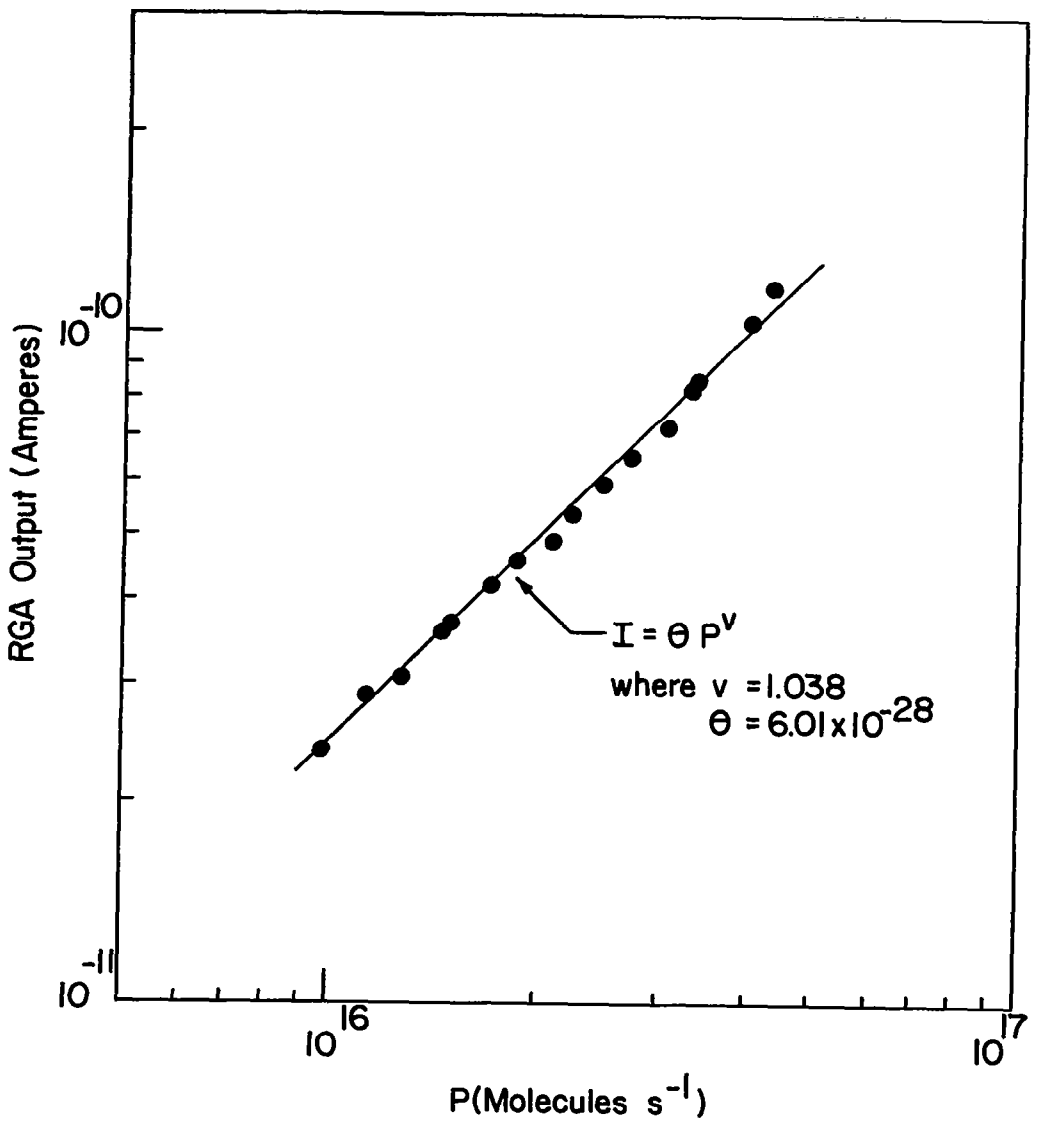

Figure 3. - Typical RGA calibration curve

TABLE II. - continued

Specimen	T (°C)	p_a (Nm^{-2})	$[\ell n(b/a)]^{-1}$	$P_o \times 10^{-20}$ (molecules s^{-1})	Q_p (J $mole^{-1}$)
1B	588-633	5.33		2.49	82,580
2A	522-640	5.33	4.24	1.15	66,850
2B	520-625	5.33		1.73	70,906
9A	595-642	5.33	2.94	2.29	75,730
9B	589-672	5.33		3.70	80,450
11B	575-643	5.33	1.79	2.16	78,880

TABLE III. - PERMEATION RATE AT 5.33 Nm^{-2} AND 600°C

Specimen	b	a	$[\ell n(b/a)]^{-1}$	P(mole s^{-1}) X 10^9	P(molecules s^{-1}) X 10^{-15}
7S5	.489	.254	1.53	12.1	7.3
11B	.489	.279	1.79	6.8	4.1
1B	.489	.305	2.12	4.6	2.8
9B	.489	.348	2.94	9.4	5.7
2B	.489	.386	4.24	16.3	9.8
1AS2	.489	.437	8.92	20.8	12.5
4A	.370	.320	6.94	23.9	14.4
2A	.405	.320	4.24	19.0	11.5
9A	.450	.320	2.94	11.2	6.7
1A	.513	.320	2.12	7.3	4.4
11A	.560	.320	1.79	5.5	3.3
3S4	.619	.320	1.52	11.6	7.0

Temperature and pressure dependence - The data for sample 4S2 from Table II are plotted in Figure 4 to illustrate the effect of temperature and pressure on the rate of permeation. As can be seen in the figure, the permeation is a direct function of the first power of the pressure. First power pressure dependence is also illustrated in Figure 5 according to equation (5b) where n = 0.982.

Geometry dependence - Figure 6 shows the combined effect of temperature and geometry at constant pressure on the permeation rate. In general, the permeation rate is highest for high values of $[\ell n\ (b/a)]^{-1}$ and lowest for low values of the same function. Based on equation (1), such a dependency would suggest that the diffusion term (last term of denominator) is partially controlling the transport process. That the transport is not totally controlled by diffusion is seen in Figure 7. A plot of permeation rate versus $[\ell n\ (b/a)]^{-1}$ according to equation (3) is linear if diffusion alone controls the transport. The

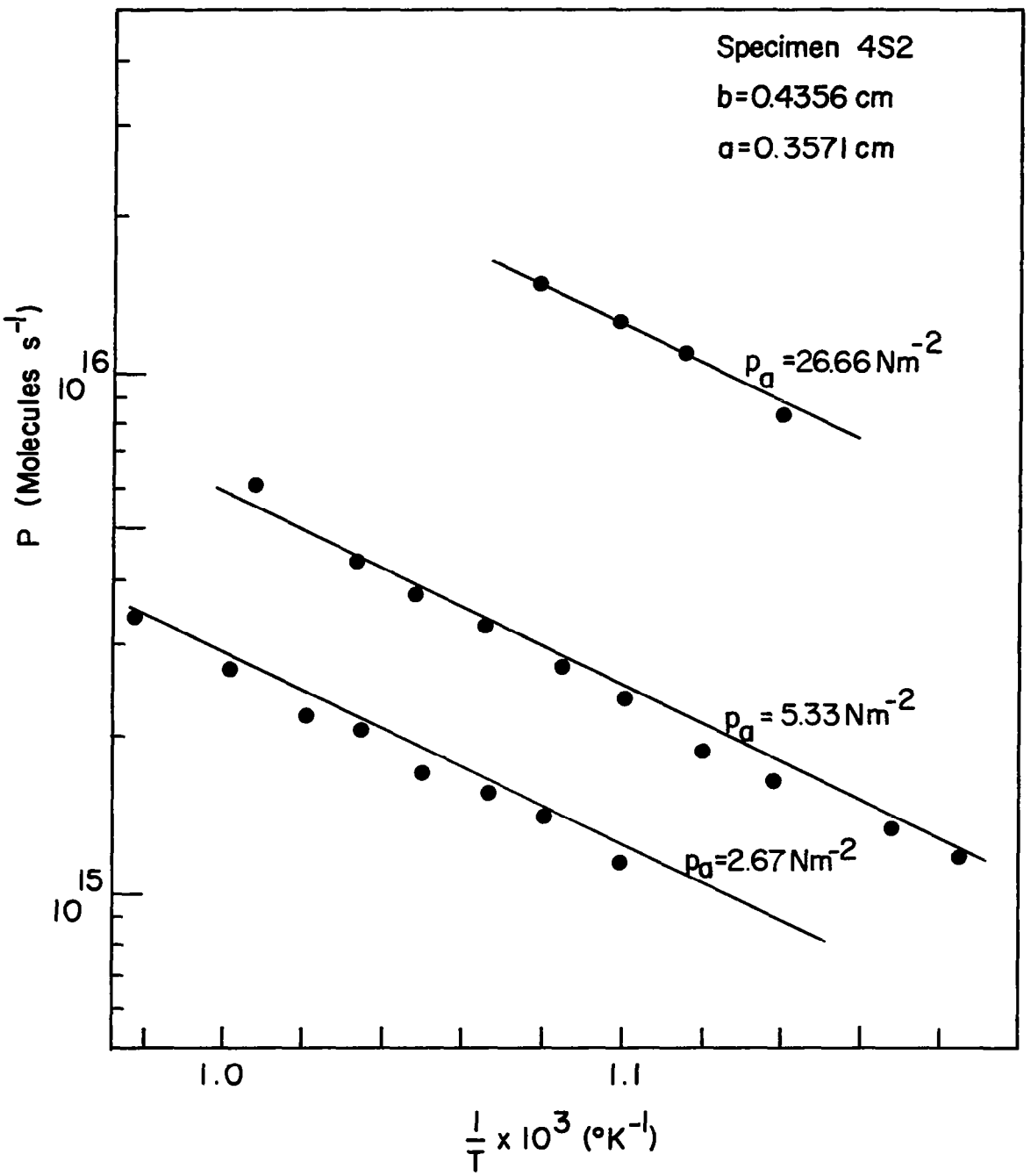

Figure 4. - Effect of temperature on the permeation rate as a function of hydrogen pressure

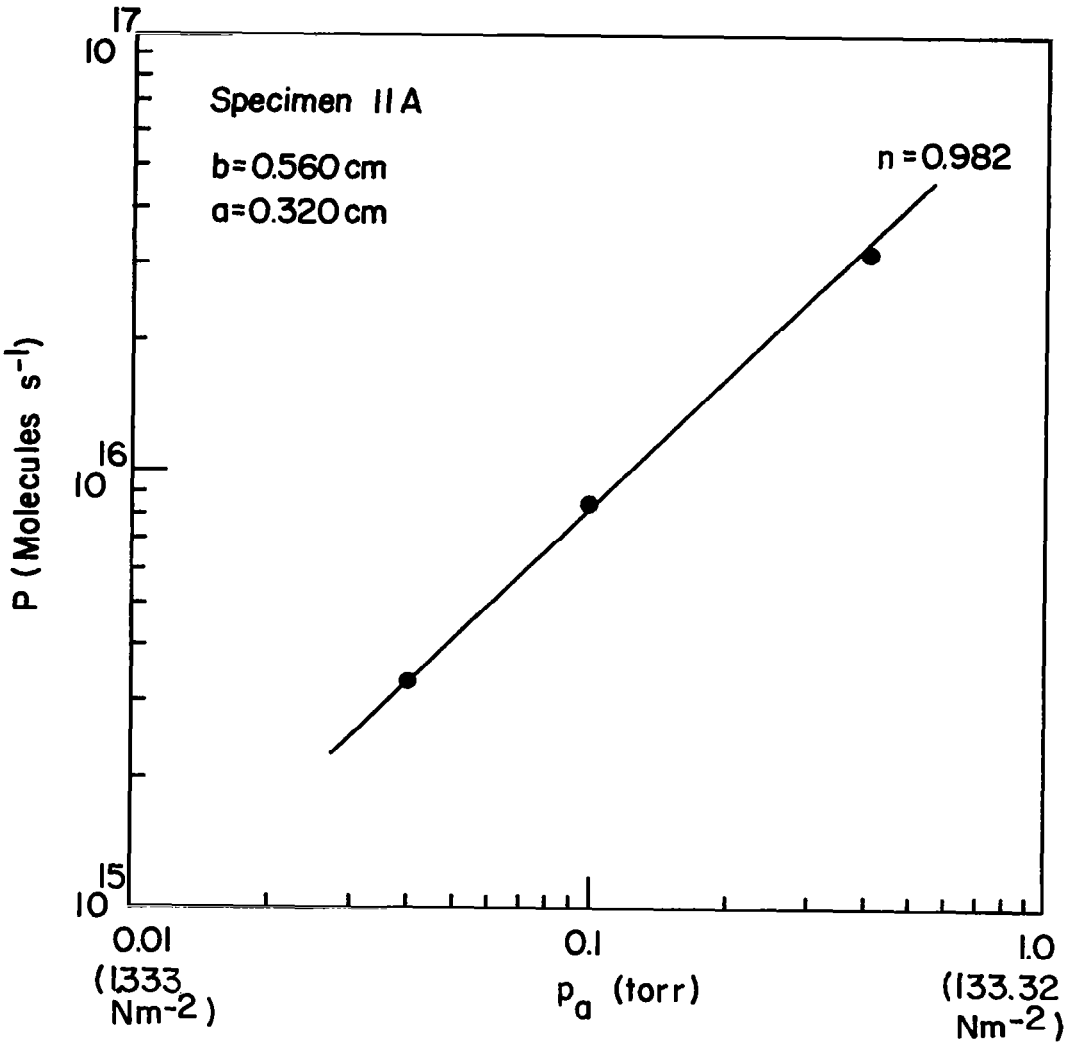

Figure 5. - Permeation rate versus hydrogen partial pressure at 600°C

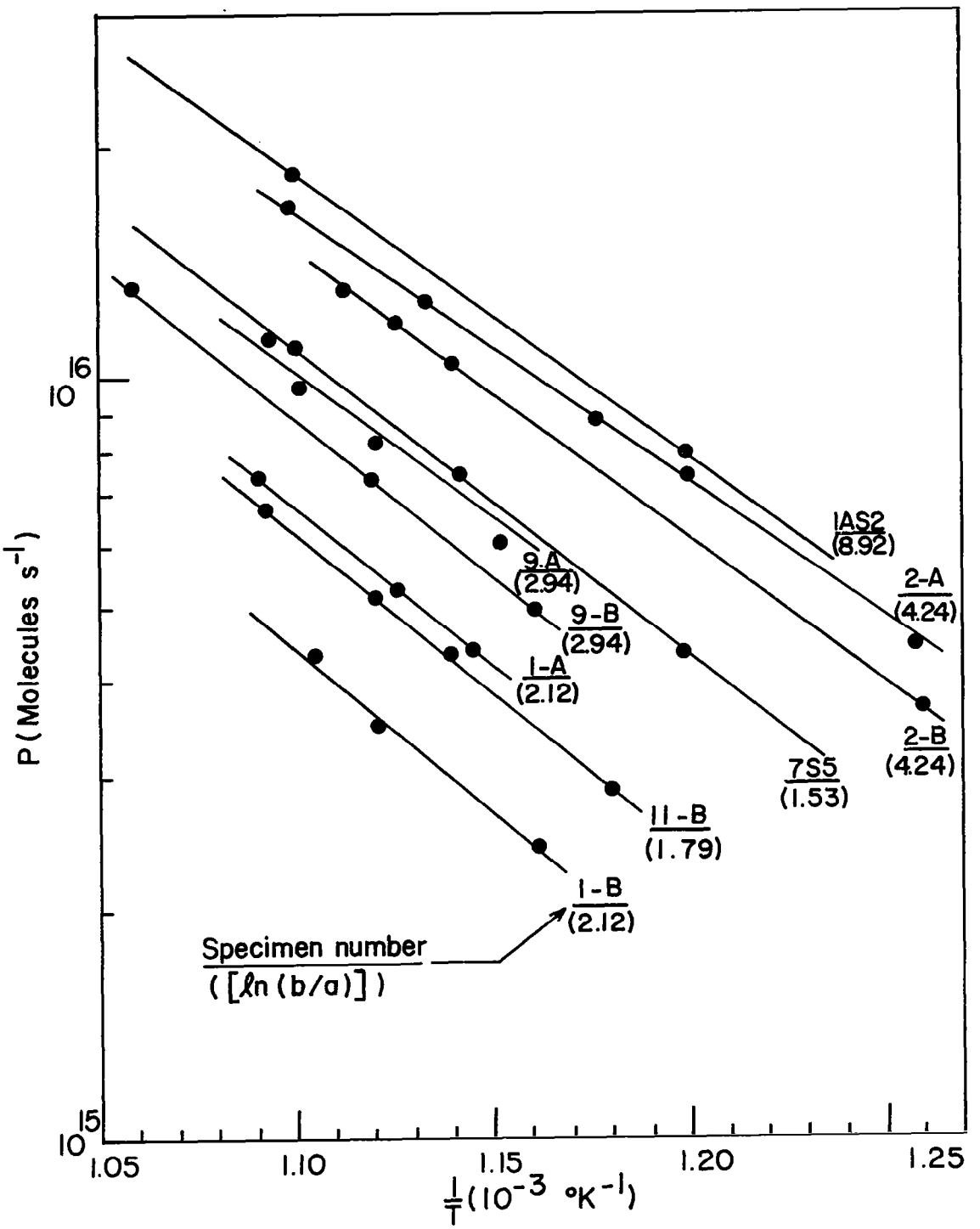

Figure 6. - Effect of specimen geometry on the permeation rate as a function of temperature at 5.33 Nm^{-2}

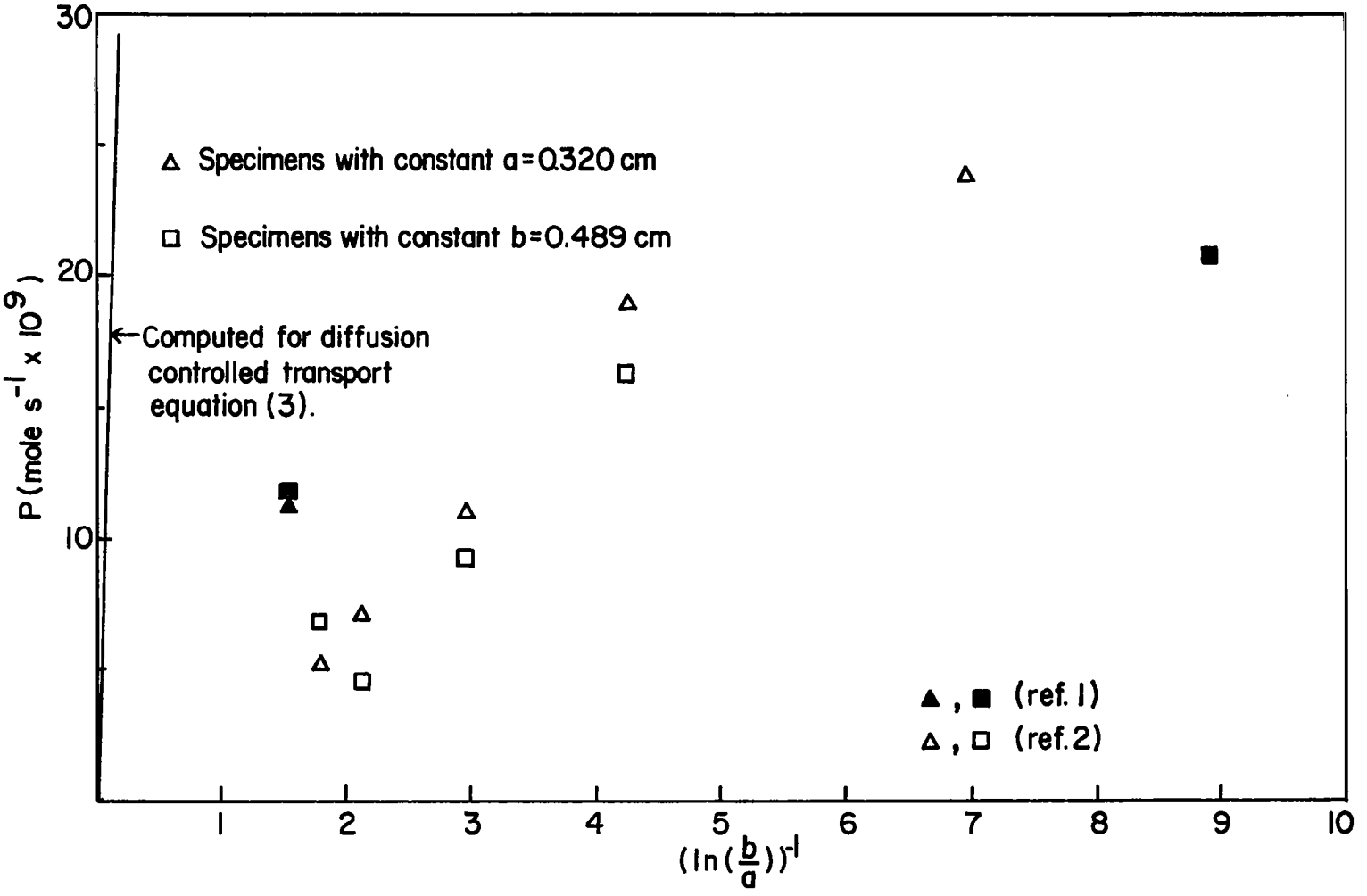

Figure 7. - Effect of specimen geometry on the permeation rate at 5.33 N/m^2 and 600°C

profile in Figure 7 is not linear, thus diffusion alone cannot control the transport. The nearly vertical line to the left of the figure shows where the points would lie if transport were purely diffusion controlled. Figures 8 and 9 show that each surface exerts partial control since the permeation rate varies when either interior or exterior radius varies and the other is held constant. Additionally, specimens with the same b/a ratio but different values of a and b yield different values of the permeation rate. This can be the case where diffusion is only partially controlling.

Effect of oxide and nitride films - After taking measurements in the "as polished" condition, selected specimens were oxidized or nitrided in situ with pure oxygen or nitrogen at 1 X 10^5 Nm^{-2} gas pressure and 270°C for times required to achieve pre-determined thickness. Film thickness was estimated from kinetic data available for flat plate specimens (refs. 25,26,27). The term "as polished" refers to membranes not pre-oxidized or pre-nitrided prior to permeation testing.

Oxide film on the interior membrane surface reduces the permeation compared with the "as polished" surface as shown in Figure 10. However, there is no change in the first power pressure dependence that was observed for "as polished" membranes. Additionally, it is significant that the location of the pre-oxidized film is critical in its effects on the permeation. Whereas oxide film on the interior surface reduces permeation, oxide film of about the same thickness on the exterior surface increases permeation somewhat. The activation energy for permeation through a specimen pre-oxidized on the interior (48A thick) is about 99,000 J $mole^{-1}$ whereas the activation energy through a specimen pre-oxidized on the exterior (34A thick) is about the same as for an "as polished" membrane or 71,000 J $mole^{-1}$. Apparently, oxide film at the interior surface has some influence on the rate controlling process. Above about 600°C, permeation rate is nearly the same as an "as polished" membrane is at the same temperature. The reason for this is probably related to the solubility kinetics of surface oxide on titanium. Above about 600°C it has been observed elsewhere (ref. 28) that the oxide film begins to dissolve in the bulk, and its effect as a surface barrier to hydrogen penetration is reduced or eliminated.

Very thin nitride films (<10A) on the interior surface of titanium reduce the permeation rate by an order of magnitude. The effect of relatively thick nitride films is shown in Figure 11. The break in the curves at 600-700°C may be due to solubility effects similar to that observed for oxide. Nitriding at the exterior surface has virtually no effect on the permeation rate as compared to the interior surface.

Diffusion

Extrapolation of the linear portion of a lag time profile is illustrated in Figure 12. Lag times determined from such profiles were used to compute diffusivity between 250-600°C. Figures 13, 14, and 15 are Arrhenius plots of the diffusivity calculated from thin, intermediate and thick membranes for the three cases of 1) Diffusion control, 2) Interior surface control, and 3) Exterior surface control. These three cases are defined by equations (9), (11),

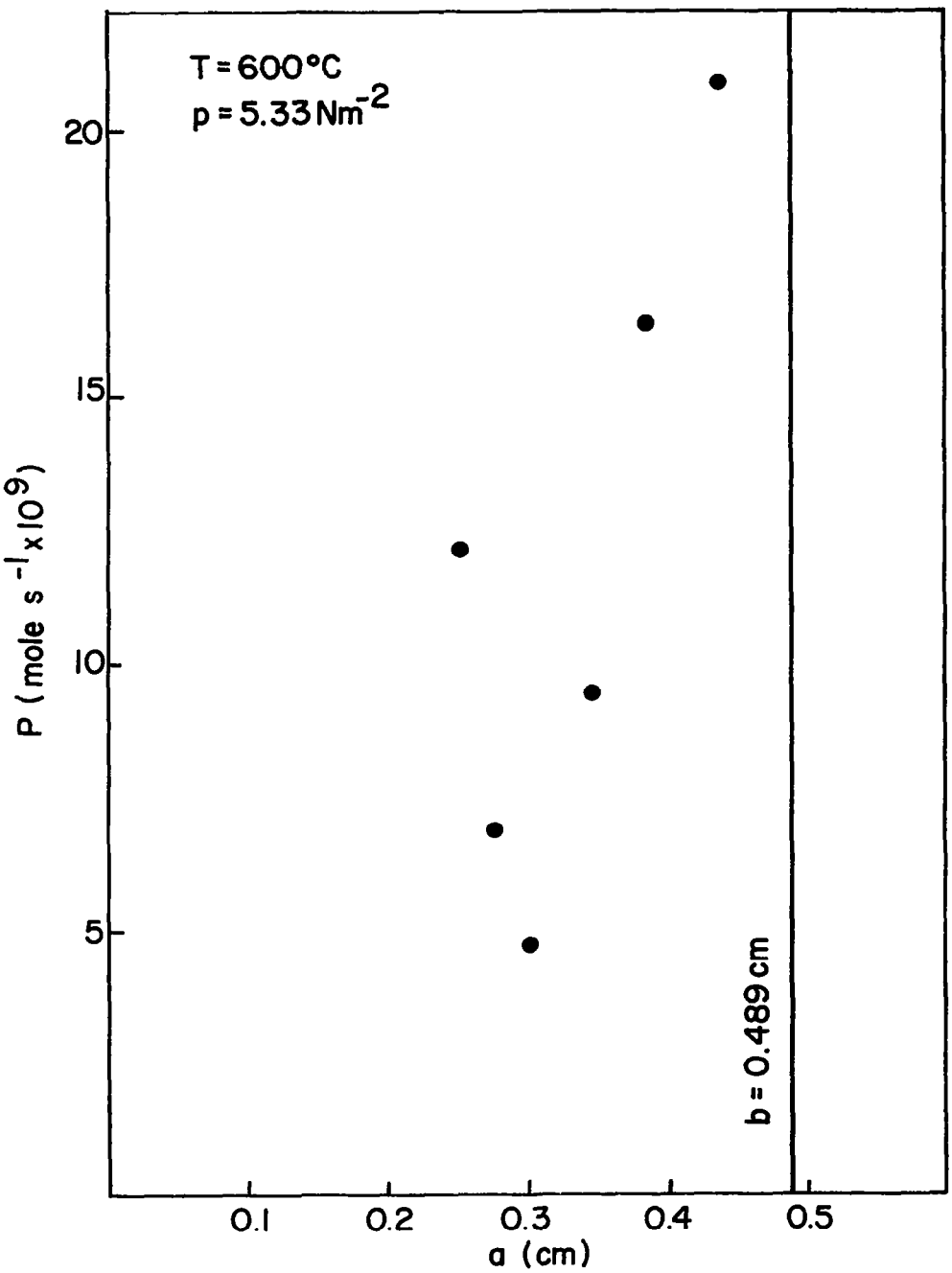

Figure 8. - Permeation rate as a function of interior radius at constant exterior radius

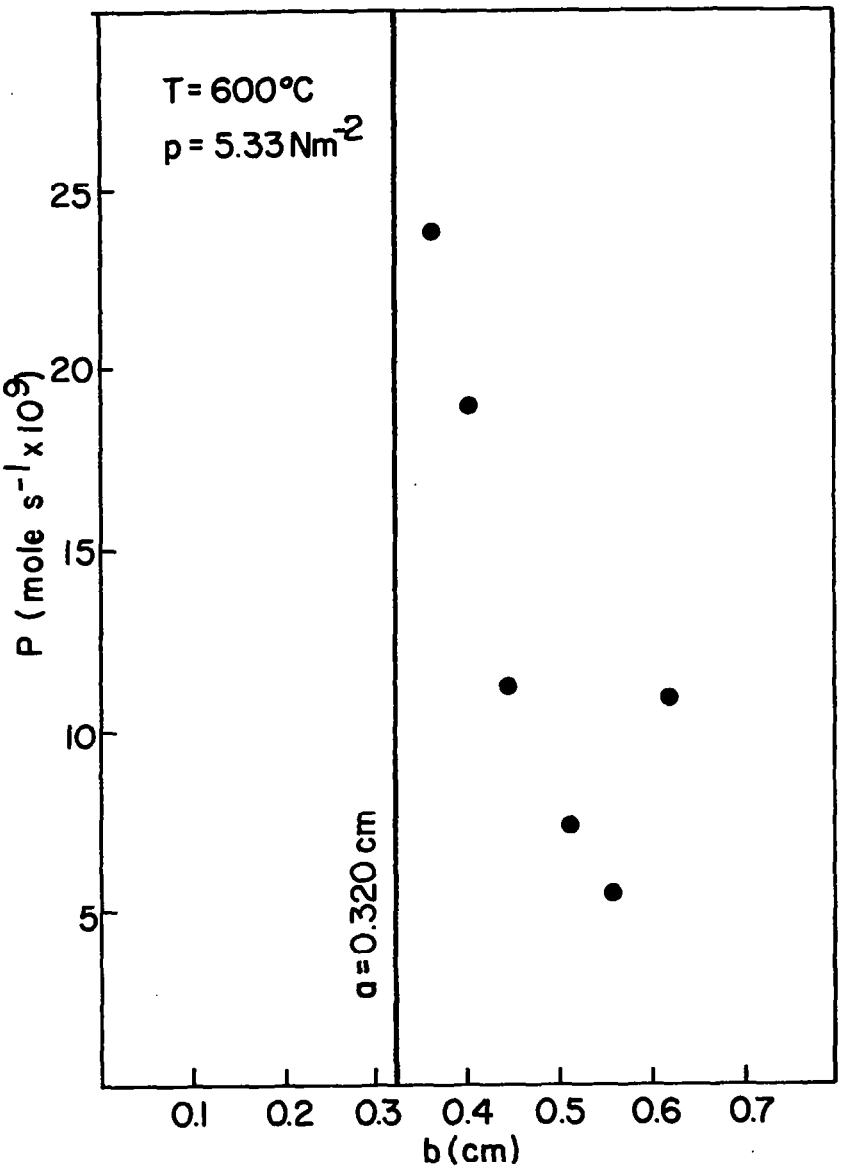

Figure 9. - Permeation rate as a function of exterior radius at constant interior radius

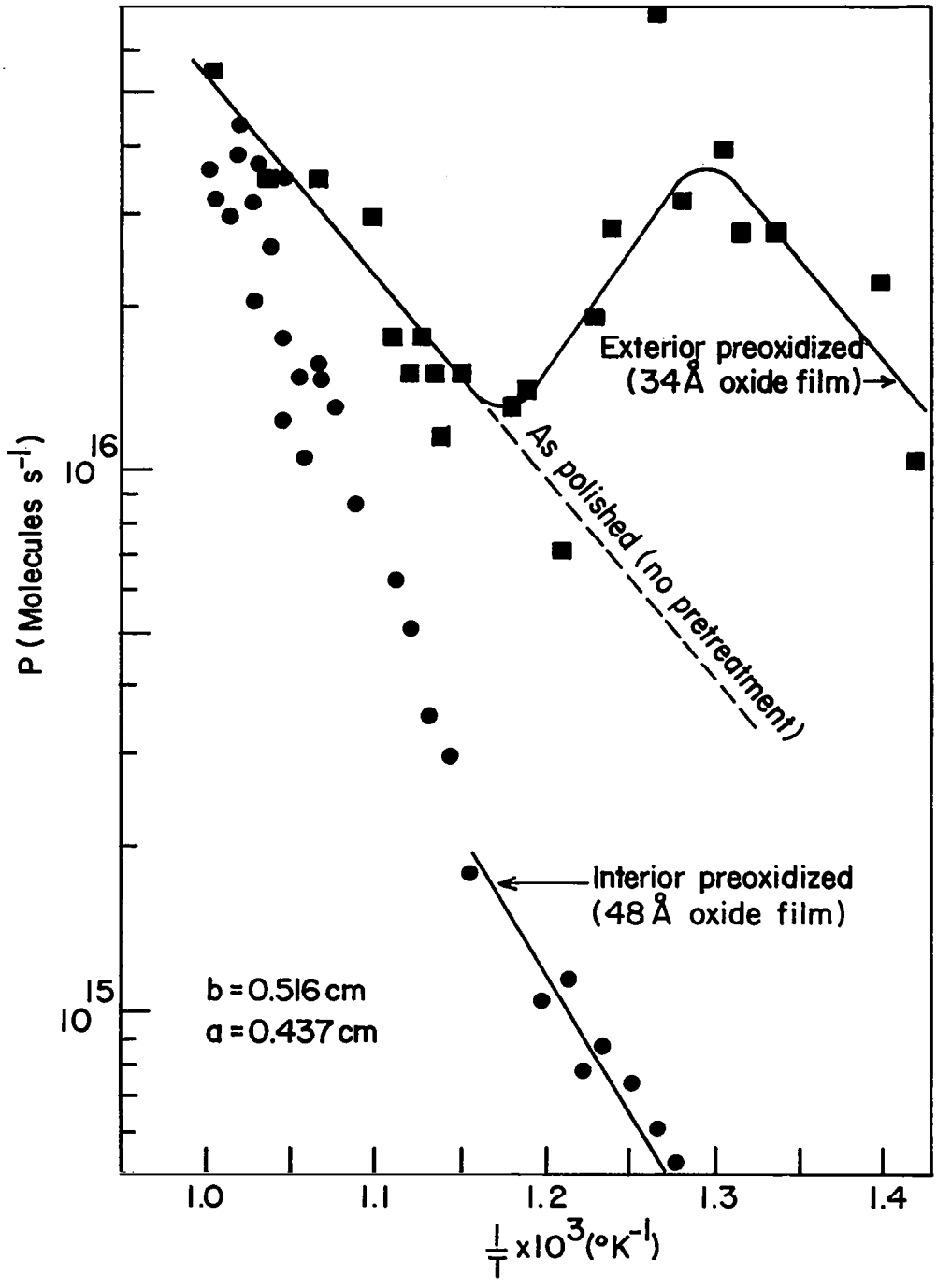

Figure 10. - Effect of surface oxide films on permeation rate as a function of temperature at 26.66 Nm^{-2} hydrogen pressure

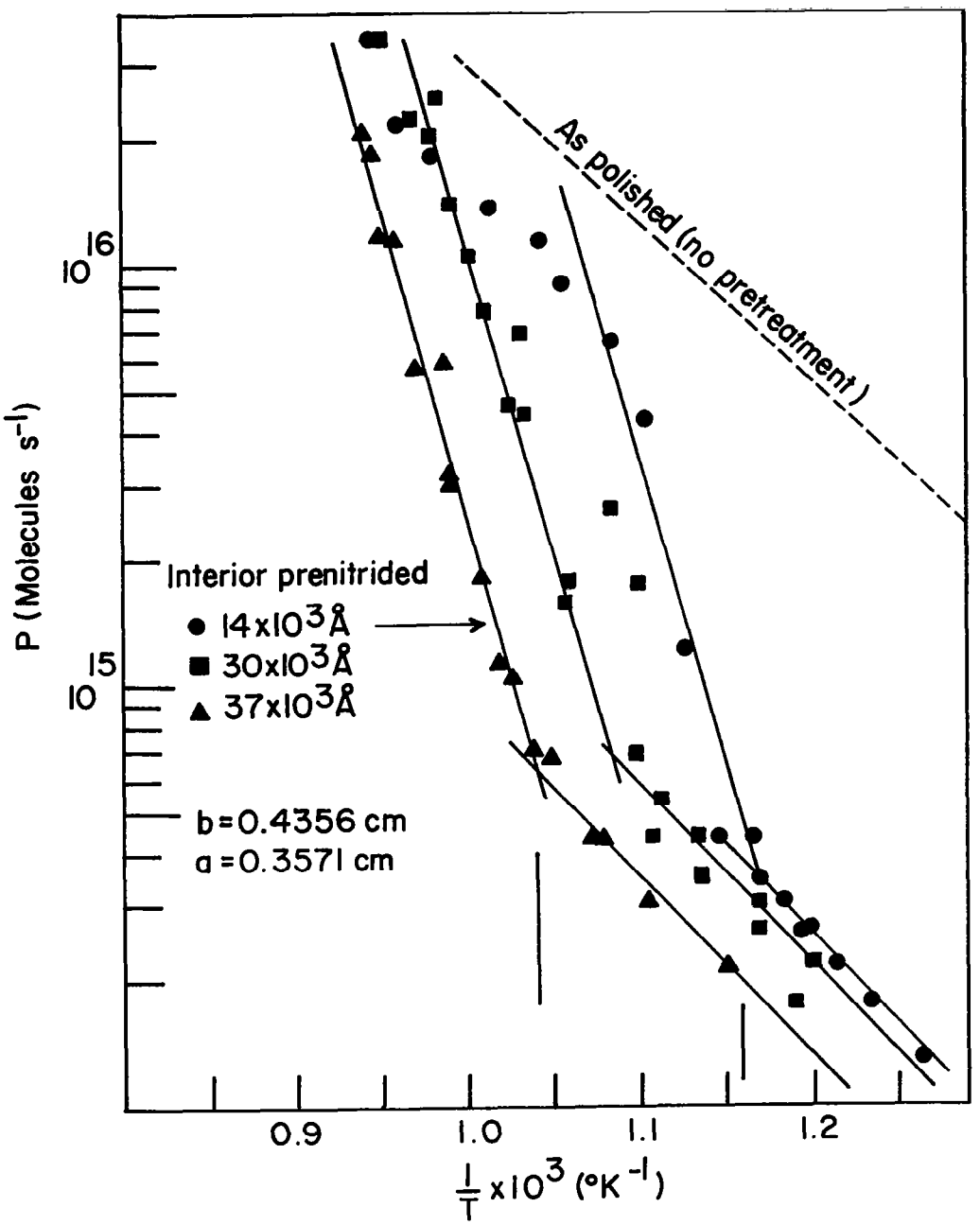

Figure 11. - Effect of surface nitride films on permeation rate as a function of temperature at 26.66 Nm^{-2} hydrogen pressure

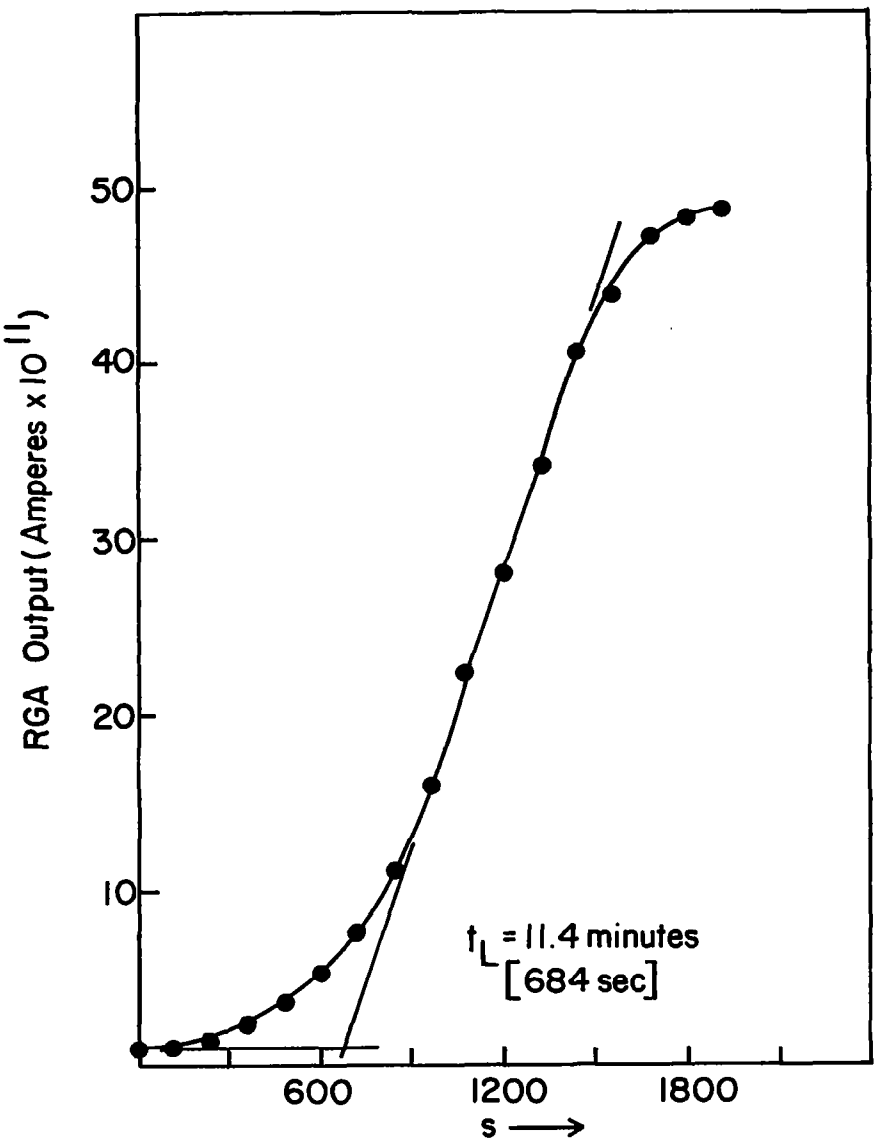

Figure 12. - Typical lag time experimental plot of current versus time at 532°C and 26.6 Nm^{-2}

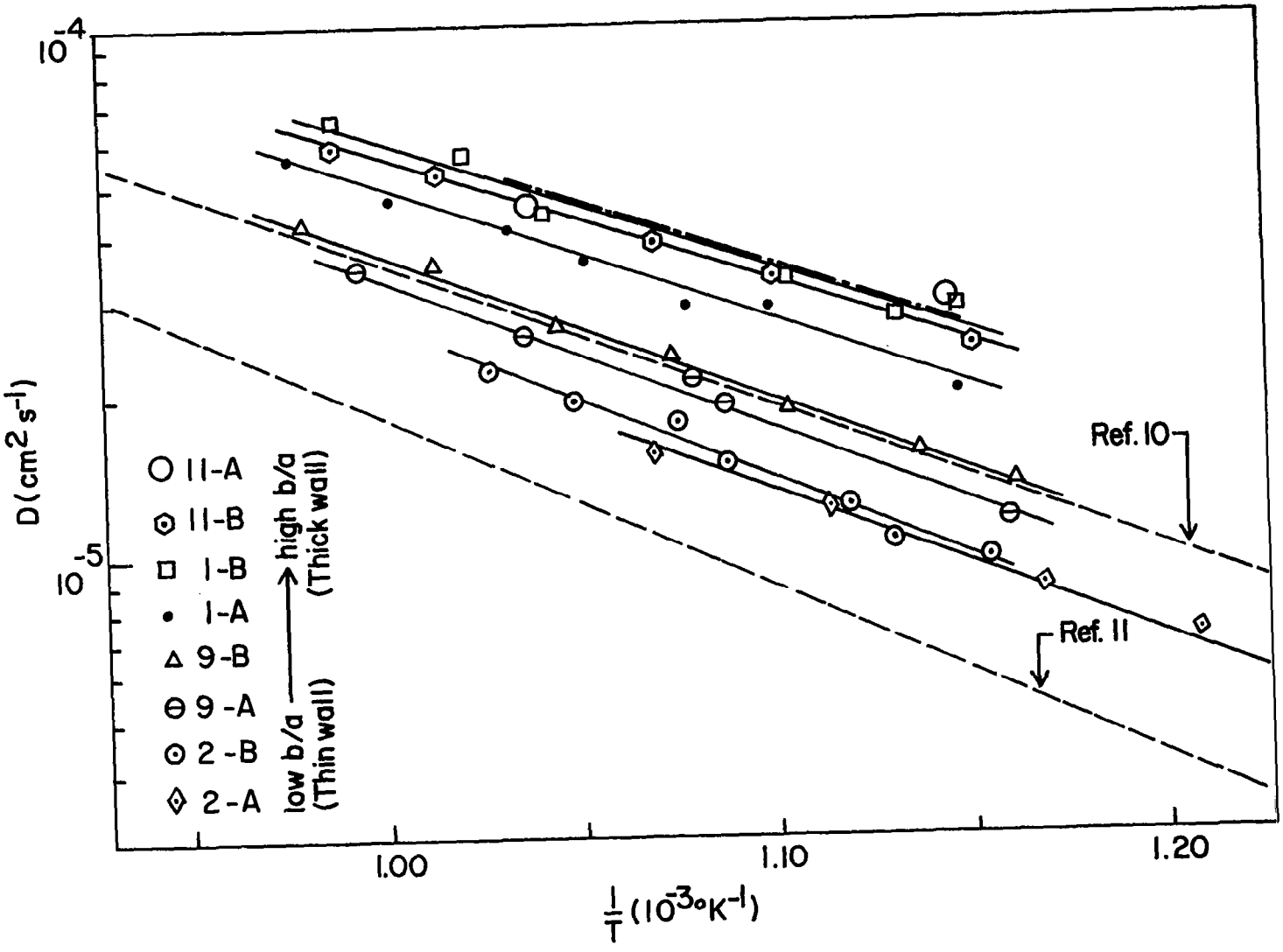

Figure 13. - Interior surface controlled diffusivity as a function of reciprocal temperature according to equation (11).

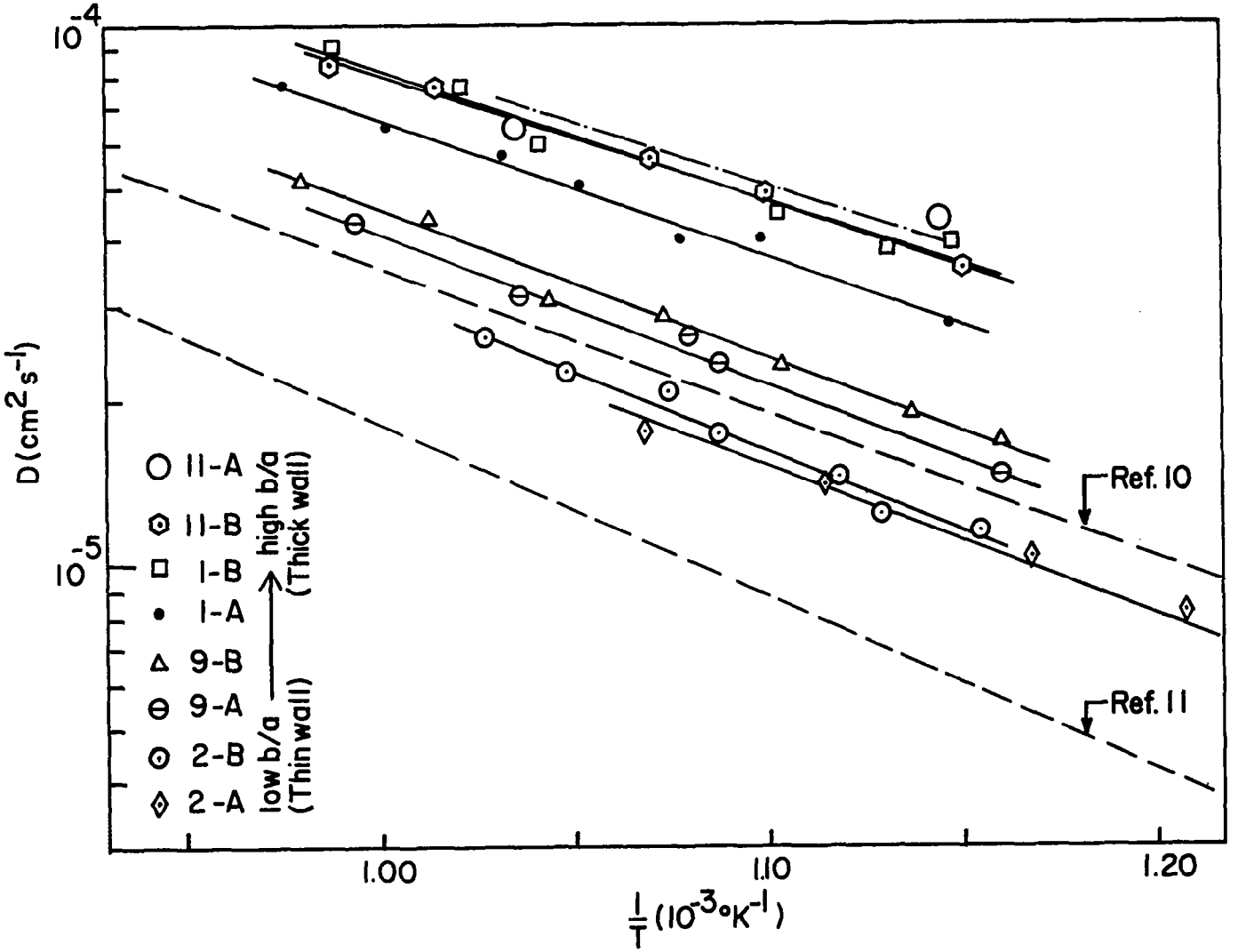

Figure 14. - Exterior surface controlled diffusivity as a function of reciprocal temperature according to equation (13).

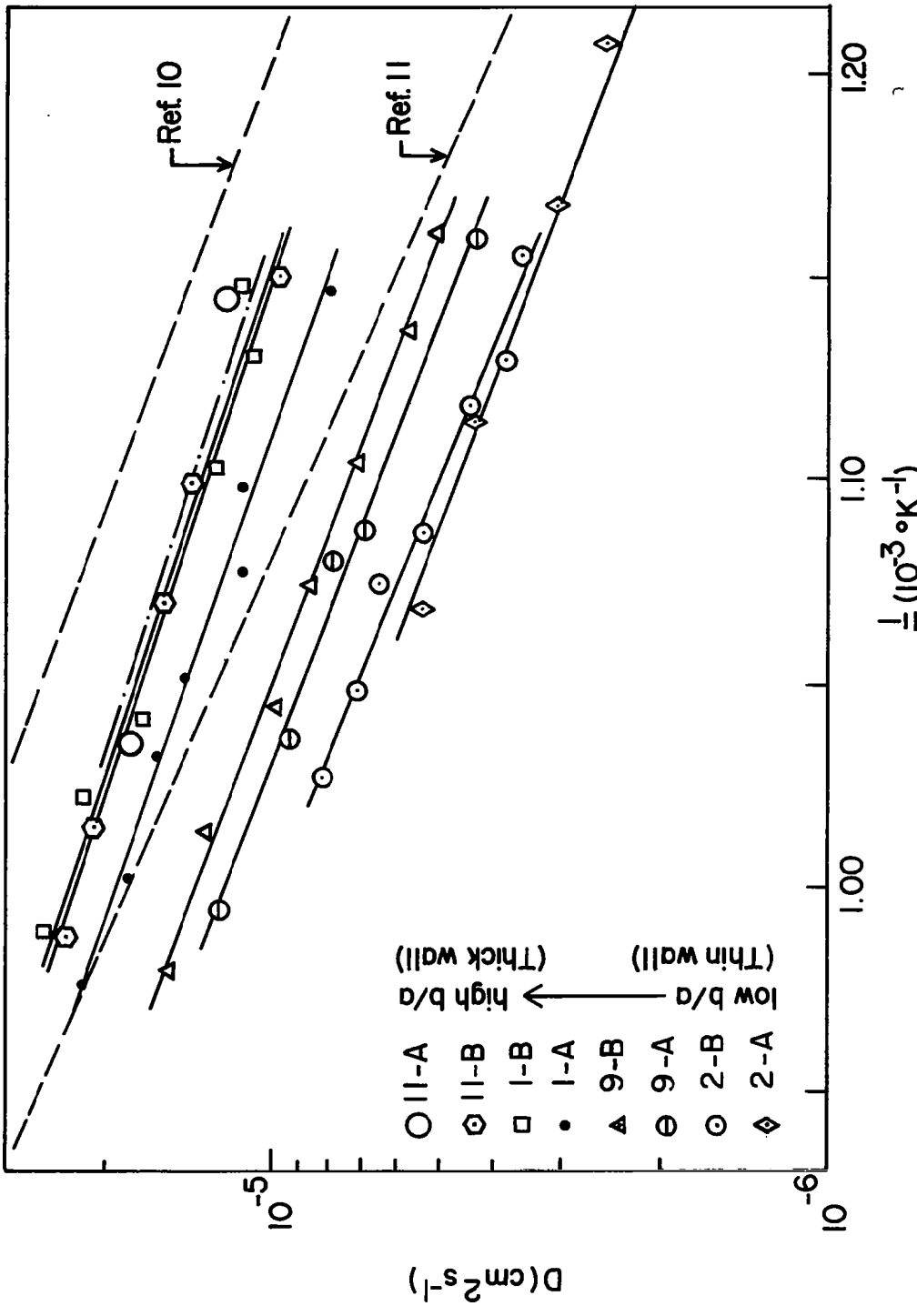

Figure 15. - Lattice controlled diffusivity as a function of reciprocal temperature according to equation (9).

and (13) respectively. For comparison, diffusion coefficient data obtained by other investigators (refs. 10,11) are superimposed on these figures as dotted lines. Based on analysis of the three figures, equation (9) gives the best fit for thick membranes (high b/a ratio) when compared with others (refs. 10,11) whereas equations (11) and (13) give the best fit for thin membranes (low b/a ratio). Thus it can be seen from diffusion data that transport is controlled by surface reactions for thin membranes and a gradual shift toward diffusion control occurs as the b/a ratio increases. This is to be expected because surface resistance becomes negligible compared to diffusion resistance as the wall thickness increases and the concentration gradient becomes negligibly small. Diffusion data corresponding to Figures 13, 14 and 15 are presented in Tables IV, V, and VI respectively.

TABLE IV. - HYDROGEN DIFFUSION PARAMETERS BASED ON INTERIOR SURFACE PHASE BOUNDARY REACTION CONTROL ACCORDING TO EQUATIONS (11) AND (12)

Specimen	T (°C)	$\frac{1}{\alpha_a}$ (cm^2)	D_o(cm^2/sec)	Q_D(j $mole^{-1}$)
1-A	599-750	.01603	1.76 X 10^{-2}	48,910 ± 2960
1-B	598-738	.01459	1.53 X 10^{-2}	46,110
2-A	533-663	.003352	1.38 X 10^{-2}	52,670
2-B	592-700	.004899	2.66 X 10^{-2}	57,130
9-A	589-732	.007519	2.15 X 10^{-2}	53,840
9-B	588-747	.008903	2.09 X 10^{-2}	52,790
11-A	600-692	.02415	1.60 X 10^{-2}	46,000
11-B	596-738	.01841	1.38 X 10^{-2}	45,950

TABLE V. - HYDROGEN DIFFUSION PARAMETERS BASED ON EXTERIOR SURFACE PHASE BOUNDARY REACTION CONTROL ACCORDING TO EQUATIONS (13) and (14)

Specimen	T (°C)	$\frac{1}{\alpha_b}$ (cm^2)	D_o(cm^2/sec)	Q_D(j $mole^{-1}$)
1-A	599-750	.02192	2.4 X 10^{-2}	48,910 ± 2960
1-B	598-738	.01995	2.1 X 10^{-2}	46,110
2-A	533-663	.003922	1.62 X 10^{-2}	52,670
2-B	592-700	.005733	3.13 X 10^{-2}	57,130
9-A	589-732	.009423	2.68 X 10^{-2}	53,840
9-B	588-747	.01116	2.62 X 10^{-2}	52,790
11-A	600-692	.03496	2.31 X 10^{-2}	46,000
11-B	596-738	.02664	1.99 X 10^{-2}	45,950

TABLE VI. - HYDROGEN DIFFUSION PARAMETERS BASED ON DIFFUSION CONTROLLED TRANSPORT ACCORDING TO EQUATIONS (9) AND (10)

Specimen	T (°C)	$\frac{1}{\alpha_D}$ (cm^2)	D_o(cm^2/sec)	Q_D(j $mole^{-1}$)
1-A	599-750	.006324	6.85 X 10^{-3}	48,910 ± 2960
1-B	598-738	.005673	5.76 X 10^{-3}	46,110
2-A	533-663	.001208	4.98 X 10^{-3}	52,670
2-B	592-700	.001765	9.61 X 10^{-3}	57,130
9-A	589-732	.002802	8.00 X 10^{-3}	53,840
9-B	588-747	.003318	7.80 X 10^{-3}	52,790
11-A	600-692	.009652	6.39 X 10^{-3}	46,000
11-B	596-738	.007356	5.50 X 10^{-3}	45,950

Geometry dependence is also observed by considering equations (18a),(18b), and (18c). At a particular temperature, the diffusion coefficient (refs. 10, 11) is constant, so a plot of $\ell n(1/t_L)$ versus $\ell n(1/\alpha_D)$, $\ell n(1/\alpha_a)$ or $\ell n(1/\alpha_b)$ will yield a straight line of slope -1 as shown in Figures 16, 17, and 18 respectively. Superimposed on these computed lines are the experimental data points obtained for the various geometries. As can be seen, the data points tend to merge with the calculated line at higher values of α_D^{-1} (thicker wall) for the case where diffusion is controlling the transport whereas the data points tend to merge with the calculated line at lower values of α_a^{-1} and α_b^{-1} for the two cases where surface reactions are controlling. As in the case of Figures 13, 14, and 15, the conclusion drawn from these sets of curves is that transport tends to be diffusion controlled for thick specimens and surface controlled for thin specimens.

DISCUSSION

It has been shown from both permeation and lag-time studies that hydrogen transport in alpha-titanium is partially or completely controlled by surface reactions depending upon membrane wall thickness and the composition and thickness of surface films.

A possible explanation for the decrease in the permeation rate in the presence of a pre-oxidized film on the interior surface is related to the formation of titanium hydride. It is suggested that steady state is established between gas-phase molecular hydrogen, a discontinuous layer of TiH_2 and atomic hydrogen in the titanium lattice. This steady state condition is modified by oxygen in such a way that partial filling of available chemisorbed sites by oxygen reduces the number of sites available to hydride. Therefore, the actual concentration of hydrogen at either the interior or exterior surface is lower than it is for the case where the surface is not pre-oxidized. A

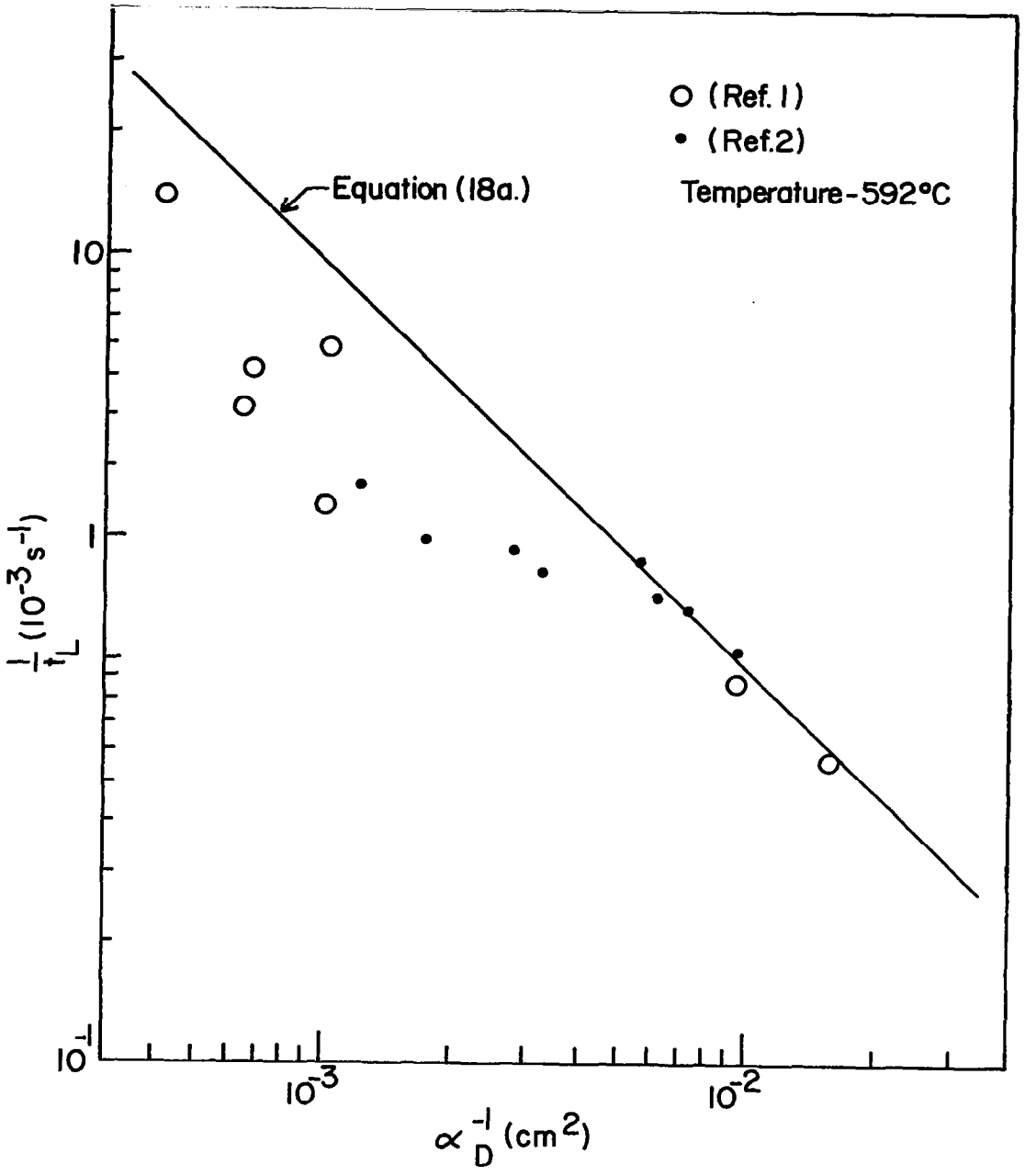

Figure 16. - Reciprocal lag time versus geometric configuration parameter at 592°C for lattice diffusion control

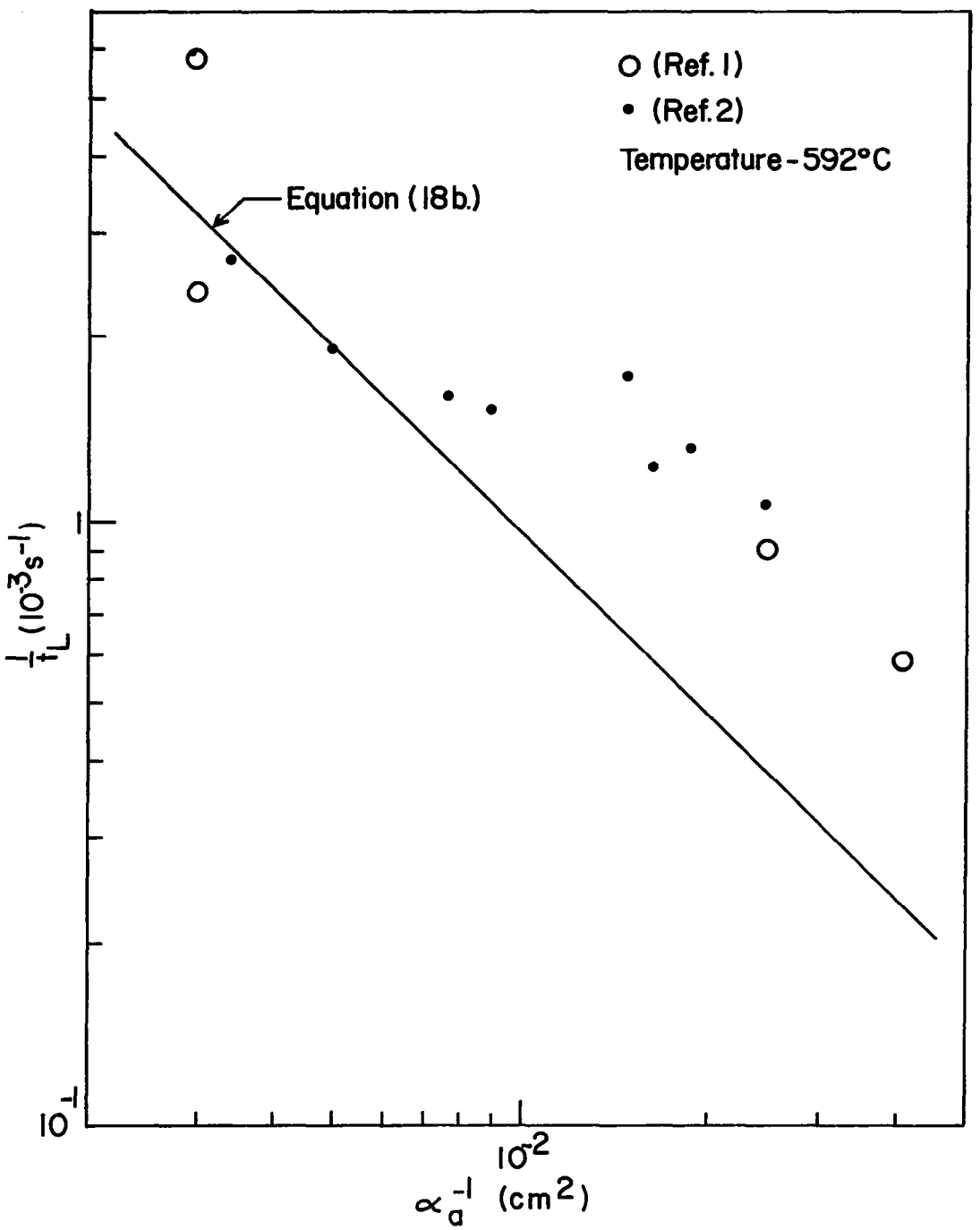

Figure 17. - Reciprocal lag time versus geometric configuration parameter for interior surface reaction control

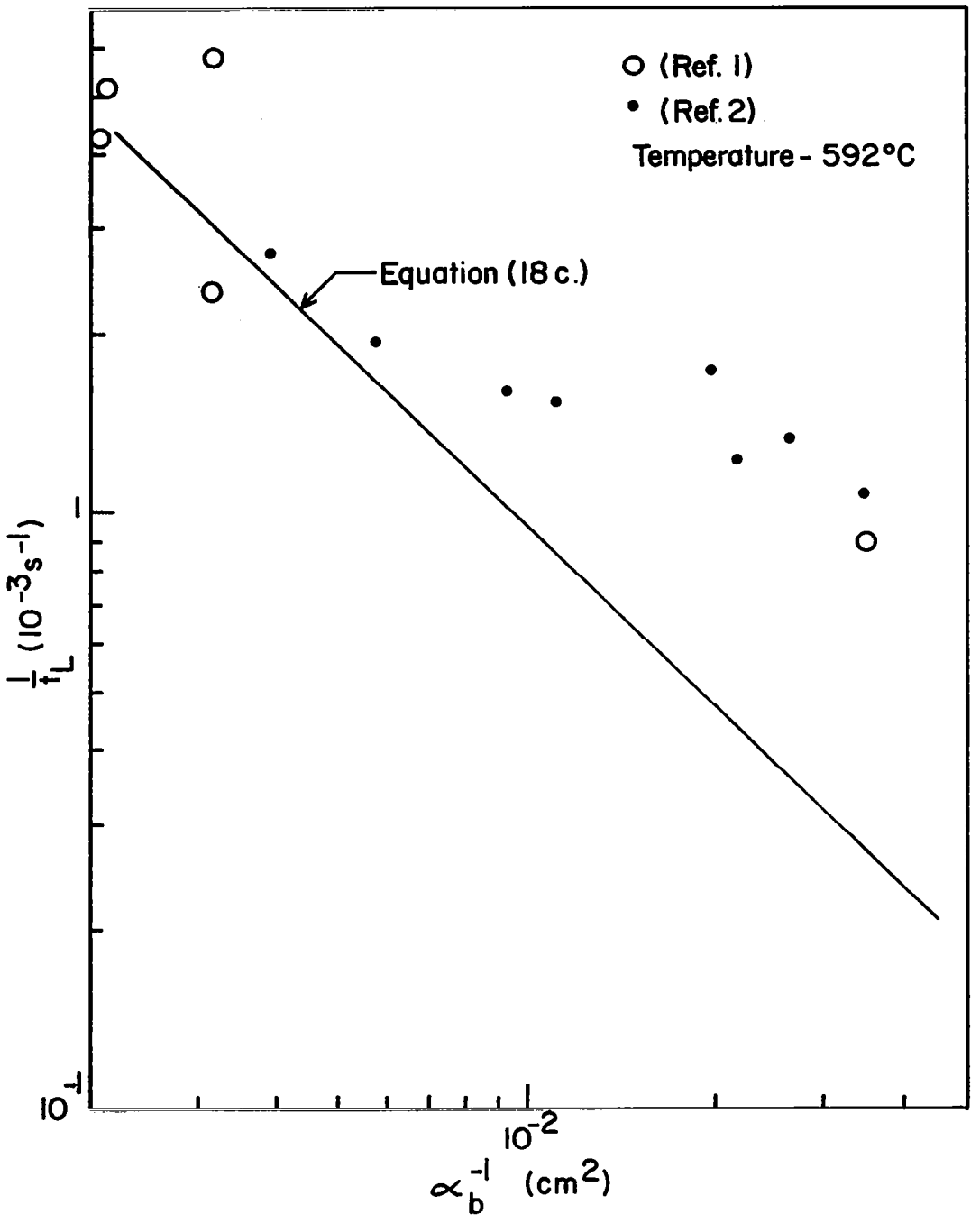

Figure 18. - Reciprocal lag time versus geometric configuration parameter at 592°C for exterior surface reaction control

decrease in concentration at the interior surface is equivalent to a reduced concentration gradient across the membrane and according to Fick's First Law, a reduced hydrogen flow rate. On the other hand, a decrease in concentration at the exterior surface is equivalent to an increased concentration gradient across the membrane and an increase in the hydrogen flow rate. Gradients developed by "as polished," interior pre-oxidized and exterior pre-oxidized surfaces are characterized in Figure 19. This interpretation of the interaction of oxide and hydride is consistent with our results in Figure 10 which show that the permeation rate is higher after pre-oxidation of the exterior surface whereas it is lower after pre-oxidation of the interior surface. Other information which adds credibility to this explanation is noted in the literature. Caskey interprets lack of hydride formation on titanium as due to the formation of a stable oxide film (ref. 16). Reichardt comments on the inhibiting effect of contaminants on reaction between hydrogen and titanium (ref. 17) and Schoenfelder and Swisher account for their results in terms of the retarding effect of oxide films on the rate of hydriding (ref. 8). Wasilewski and Kehl also recognized the effect of oxide on reaction rates in titanium (ref. 10).

A comparison of D_0 values in Table VI with that in Tables IV and V shows that the former are lower by a factor of about three. Since the D_0 values in Tables IV and V are in good agreement with the results reported by others (refs. 10,11), it appears that equations (9) and (10) give a result that is too low and in error by a factor of three. Phillips and Dodge (ref. 20) predicted similar findings for type 321 stainless steel and noted that if one is not aware that surface processes are affecting the measurements, the value of D calculated from lag-time measurements according to equations (9) and (10) could be as much as three times too small. Quick (ref. 29) notes that when hydrogen diffusivities in iron associated with surface impedance are multiplied by a factor of three or less, they correspond closely with volume controlled diffusivity. The factor of three noted by Phillips, Dodge and Quick appear to be readily explainable if it is assumed that phase boundary reactions limit the permeation of hydrogen. As discussed above, the same observations were made with regard to alpha titanium.

CONCLUSIONS

Hydrogen transport through alpha-titanium is a complex process involving simultaneous diffusion and phase boundary reactions at both inlet and outlet surfaces. The relative effect of each surface depends upon the extent of surface contamination as well as physical dimensions of the membrane.

Permeation

Steady state hydrogen permeation through alpha titanium in the "as polished" state in contact with atmospheric air is dependent upon the first power of the input hydrogen pressure. As a result, permeation cannot be expressed in terms of a simple Sievert's Law relationship as can be done for less reactive metals such as iron and iron base alloys. The best value of the

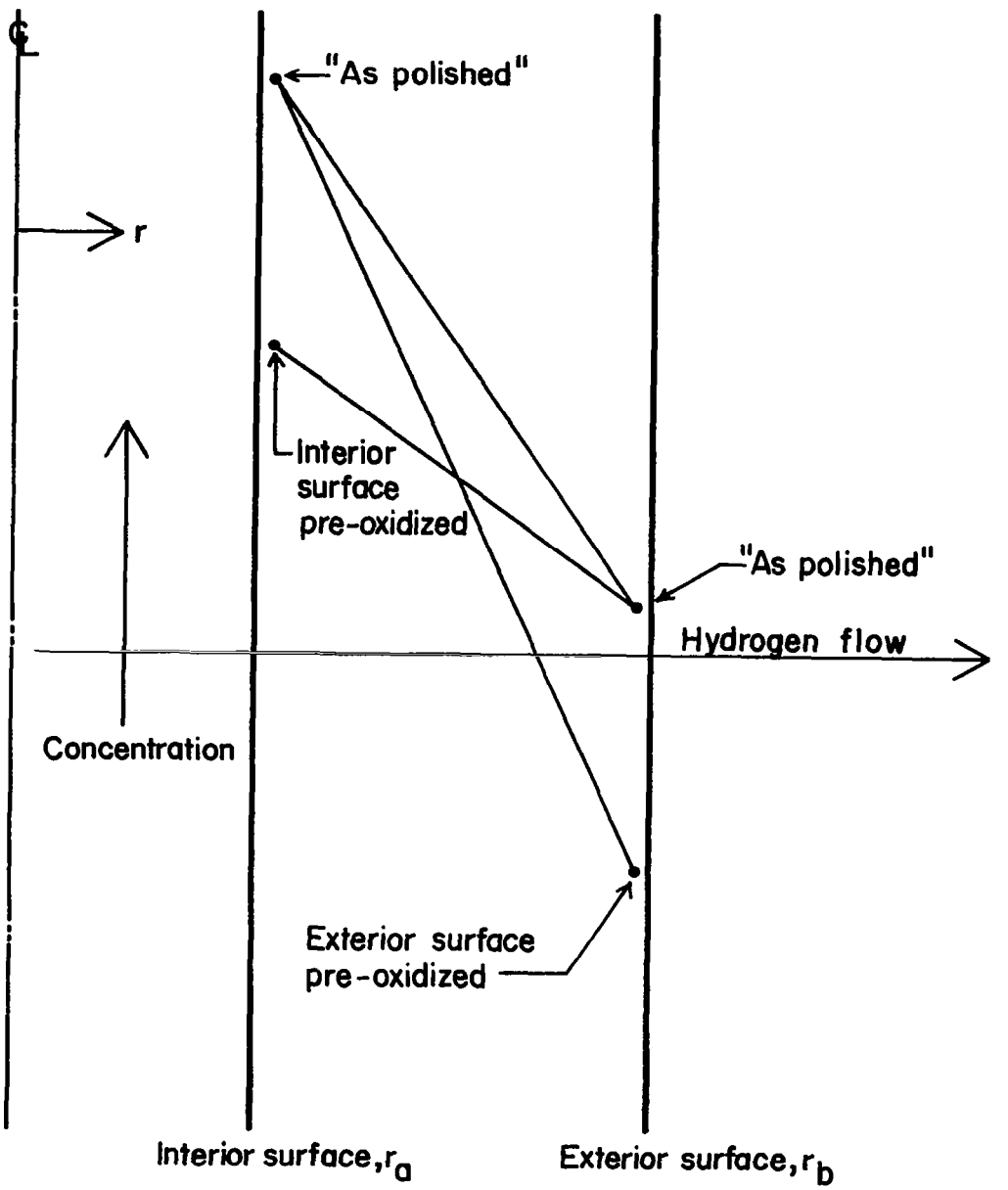

Figure 19. - Gradients across membrane for "as polished" and pre-oxidized surfaces

permeation activation energy between 400-800°C is Q_p = 74,300 Joules $mole^{-1}$. The pre-exponential constant P_o is variable between about 0.4 X 10^{20} and 2.5 X 10^{20} molecules s^{-1} at a hydrogen input pressure of 5.33 Nm^{-2} and a maximum membrane wall thickness (or equivalent b/a ratio) of about 0.3 cm. Conversion to P_o values for other pressures below 30 Nm^{-2} can be made using equation (6b). Conversion to permeation rates for other tube dimensions is best accomplished by references to Table II.

Oxide and nitride films at the hydrogen input surface tend to retard permeation by a factor of 10 or more at temperatures below 600°C. Above this temperature, the oxides and nitrides begin to dissolve in the bulk and the protective film is destroyed. In general, films located at the hydrogen outlet surface tend to increase the permeation rate in contrast to films located at the inlet surface. Permeation is first power pressure dependent regardless of whether the surface is pre-oxidized or not.

Diffusion

The diffusivity for hydrogen transport in alpha titanium is given by

$$D = 2.1 \times 10^{-2} \exp\left(\frac{-50,400}{RT}\right)$$

which is in excellent agreement with the results of others (refs. 10,11). An analysis of lag-time data reveals that unsteady state transport tends toward surface reaction control for thin (low b/a ratio) membranes and toward diffusion for thick membranes. The transition from surface to diffusion control occurs near b/a = 1.6. The presence of thin oxides and nitrides on the surface does not significantly affect the diffusion coefficient obtained by the lag-time technique.

PART II

GAS-PHASE HYDROGEN PERMEATION AND DIFFUSION IN CARBON STEELS AS A FUNCTION OF CARBON CONTENT FROM 250-600°C

Donald L. Johnson and Vijay L. Gadgeel

University of Nebraska

SUMMARY

Commercial heats of armco iron, 1010, 1020, 1035, 1050, 1065, and 1095 steel were normalized and machined into hollow cylinders. Coefficients of hydrogen permeation and diffusion were determined with a quadrupole residual gas analyzer at temperatures between 250 and 600°C and pressures between 1.013×10^5 and 4.052×10^5 Nm^{-2}. Pressure dependence measurements established that lattice diffusion was controlling transport and Sievert's law was applicable for the correlation of experimental data. The permeation coefficient for alpha iron is in good agreement with the data of Nelson and Gonzalez but decreases in the commercial steels as the carbon content increases. Hydrogen solubility and diffusivity likewise decrease as the carbon content increases. The decrease in diffusivity and solubility is explained in terms of hydrogen trapping at carbide interfaces. A comparison of diffusivity data for 1065 steel in the quench and tempered, spheroidized, and normalized condition confirms such an explanation.

INTRODUCTION

In order to develop a quantitative understanding of hydrogen attack in coal gasifier pressure vessel steels, three goals were set forth in the Ames program: 1) an understanding of the process of hydrogen entry and transport, 2) an understanding of the three stages of attack, and 3) the application of existing models of void nucleation and growth. Part II of this report is directed to goal 1) and describes the results of gas phase permeation studies in carbon steels as a function of carbon content and microstructure.

Hydrogen permeation and diffusion data for alpha iron are reviewed in several recent papers (refs. 30,31,32,33,34). The agreement among investigators is generally quite good with regard to steady state permeation but the agreement is not so good with regard to unsteady state diffusivity. Part of the reason for disagreement in diffusivity data is that the values were often computed from permeation and solubility data and were not determined by direct experiment. In this study, it was important to establish accurate base line data for alpha iron, and this was accomplished by comparing literature data considered pertinent from the standpoint of source and experimental technique.

According to Smialowski (ref. 34, pp. 64-117), the presence of carbon considerably diminishes the hydrogen permeation rate and the structural form of cementite greatly influences the permeability. Eschbach et al. (ref. 35) showed that increasing the alloy content decreased the permeability although the effect of carbon was not clear since the range of carbon contents was quite small. According to the review by Fletcher and Elsea (ref. 36, p. 50), increasing the carbon content decreased the permeation rate at room temperature considerably. At high temperatures, increasing the carbon content appears to result in an increase in the permeation rate rather than a decrease observed at lower temperatures.

According to Mindyuk and Svist (ref. 37), an increase in carbon content decreases the diffusion mobility of hydrogen in steel at temperatures between 10°C and 90°C. Eschbach et al. (ref. 35) made similar observations at temperatures up to 600°C. Angeles et al. (ref. 38) found that alloying decreases diffusivity although they did not isolate the effect of carbon. Similarly, Nelson and Stein (ref. 39) found that diffusivity decreased in 4130 steel as compared to alpha iron. According to Oriani (ref. 33), it is very difficult to determine whether much has been learned about the change of diffusivity with alloying additions due to the sensitivity to traps.

Nikonorova et al. (ref. 40) state that there is a clear tendency for the intensity of hydrogen diffusion and permeation to increase when the equilibrium annealed structure changes to metastable structures during hardening heat treatment. Nelson and Stein (ref. 39) found that the diffusivity of 4130 steel was higher in the quenched and tempered condition than in the normalized condition. Robertson (ref. 41) recently reported that steady state permeability through 1045 steel was independent of heat treatment. The apparent diffusivity varied appreciably with heat treatment and was interpreted as due to hydrogen trapping at carbide interfaces with the most trapping occurring in a material with a fine pearlite structure. Eschbach (ref. 35) found that steels with an austenitic structure showed a lower diffusivity than those with a ferritic structure. Additionally Kikuya and Araki (ref. 42) reported that ferrite-pearlite structures had higher diffusivities and solubilities than sorbite, troostite or martensite. In general, there appears to be fairly good agreement that microstructure resulting from variation in heat treatment has an effect on hydrogen diffusivity although there is no general agreement about the effect of microstructure on hydrogen permeability.

According to Smialowski (ref. 34, p. 35), measurements of the solubility of hydrogen in iron carbon alloys are complicated by the formation of methane and hence the few experimental data found in the literature are controversial. Nelson and Stein (ref. 39) show that the solubility is lower for a normalized 4130 steel than for alpha iron. A calculation from the graphs given by Nikonorova (ref. 40) shows that the hydrogen solubility decreases with increasing carbon content at temperatures between 150°C and 480°C. However, Smialowski (ref. 34, p. 35) reported increasing absorption of hydrogen with increasing carbon content in alloys with carbon in the range 0.025 - 2.64 w/oC. Yoshizawa and Yamakawa (ref. 43) also found an increase in hydrogen solubility with increase in carbon content.

Based on the results of this literature review, it was noted that experimental measurement of hydrogen transport in steels as a function of carbon chemistry at temperatures between 300°C and 600°C has not been adequately addressed, and it is precisely in this range that hydrogen attack occurs. A carefully planned experimental program was implemented to deal with two important hydrogen attack variables, namely, carbon content and heat treatment.

EXPERIMENTAL

The experimental test system, sample preparation, and procedure are similar to that used for the study of titanium in Part I. The specimens were preheated for about an hour at 500°C in low pressure hydrogen to remove surface oxide. This was followed by vacuum annealing to remove residual hydrogen.

RESULTS

Nelson and Stein (Ref. 39) demonstrated that steady state gas-phase hydrogen transport in alpha iron and 4130 steel is controlled by lattice diffusion and is not affected by surface reactions. This was confirmed in the present experiments by making measurements to determine whether or not the permeation was dependent upon the square root of hydrogen pressure according to equation (5a) and corresponding Figure 20. As can be seen in the figure, the values of n were near 0.5 with a maximum deviation of 0.024. Based on these results, it was assumed that Sievert's law was valid and equations (7), (8), (9), (10), (16), and (19) were applied to the evaluation of permeation, diffusion, and solubility parameters at pressures between 1.0×10^5 Nm^{-2} and 3.45×10^5 Nm^{-2} and temperatures between 250°C and 600°C.

Permeation

Effect of Carbon Content - The pre-exponential constant and permeation activation energy for each carbon steel alloy are presented in Table I.

TABLE I. - ARRHENIUS CONSTANTS FOR HYDROGEN PERMEATION IN ALPHA IRON AND NORMALIZED CARBON STEELS

Alloy	w/o C	$\phi_o \times 10^6$	Q_p
Armco Ingot Iron	0.008	5.633	31,690 ± 2400
SAE 1010	0.08	7.715	34,180
1020	0.23	8.450	35,070
1035	0.31	8.076	36,160
1050	0.48	4.700	34,130
1065	0.63	3.590	34,730
1095	1.23	2.328	33,430

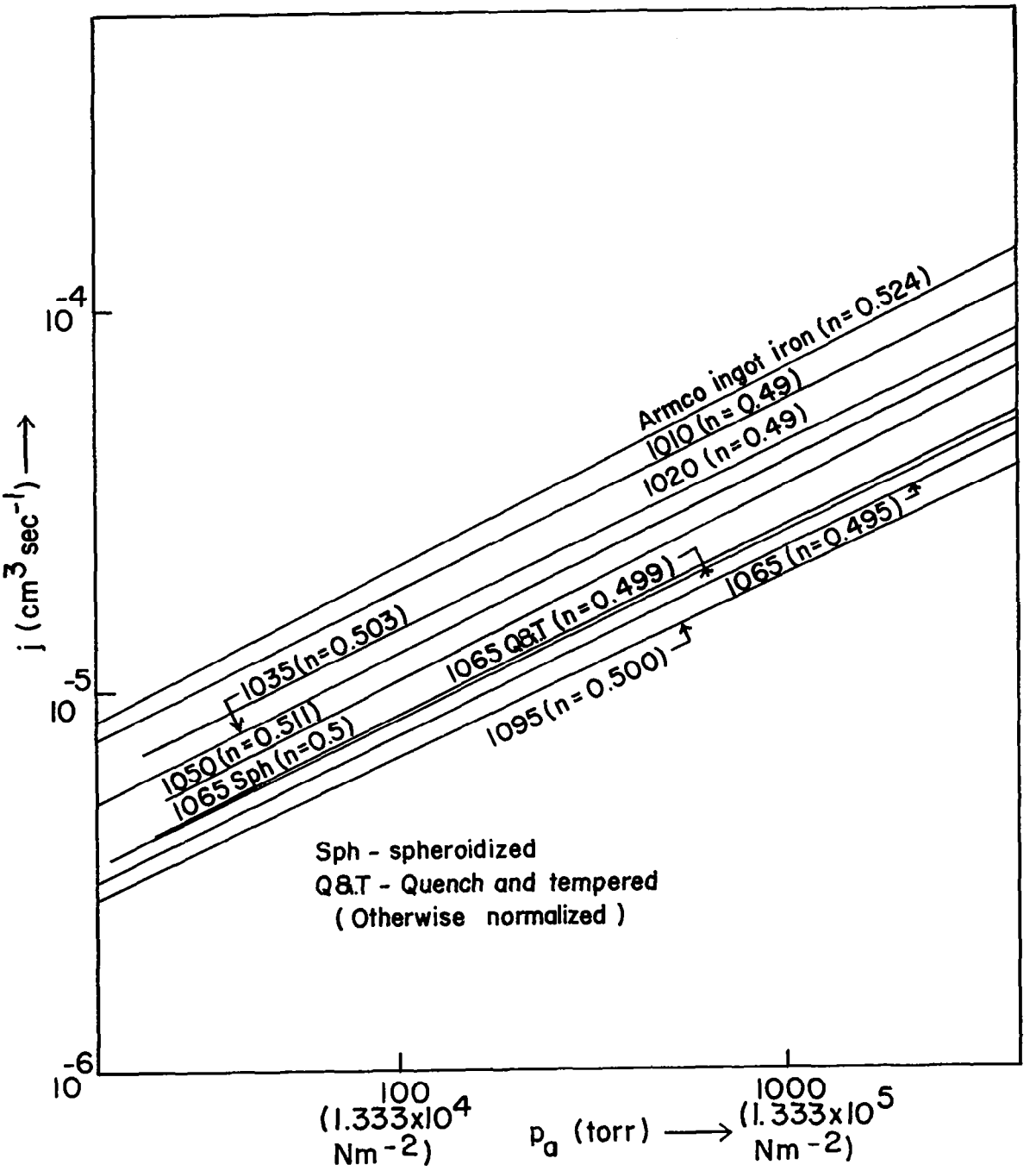

Figure 20. - Hydrogen permeation pressure dependence through alpha iron, carbon steels and heat treated 1065 steel

The corresponding coefficients of hydrogen permeation are presented in Figure 21 as a function of temperature. As can be seen in the figure, the data obtained for alpha iron are in excellent agreement with the data reported by Gonzalez (ref. 31), and Nelson (ref. 39). Additionally, Nelson's permeation data for 4130 steel are somewhat lower than 1035 steel as would be expected for an alloy containing about the same amount of carbon but with metallic alloy additions (ref. 36, p. 49). The permeation results are internally consistent and clearly indicate that permeability decreases as the carbon content increases between essentially 0 w/o carbon and about 1.2 w/o carbon. Thermally activated Arrhenius behavior is indicated throughout the carbon composition range. The permeation activation energy is independent of carbon content within experimental error as Table I shows. The permeation rate decreases primarily as a result of a decrease in the pre-exponential constant.

Effect of Heat Treatment - The pre-exponential constant and permeation activation energy for 1065 steel in the quench and tempered, spheroidized and normalized condition are presented in Table II.

TABLE II. - ARRHENIUS CONSTANTS FOR HYDROGEN PERMEATION IN 1065 STEEL AS A FUNCTION OF HEAT TREATMENT

Alloy Condition	$\phi_o \times 10^6$	Q_p
Quench and tempered	3.295	33,800 ± 2050
Spheroidized (in situ)	6.030	36,560
Normalized (in situ)	3.872	34,760

The corresponding coefficients of hydrogen permeation are presented in Figure 22 as a function of temperature. The quench and tempered and normalized structures show nearly identical permeation rates and suggest that permeation is independent of heat treatment as reported in Robertson (ref. 41). As expected, thermally activated Arrhenius behavior is indicated for all heat treatments.

DIFFUSION

Effect of Carbon Content - The pre-exponential constant and diffusion activation energy for each carbon steel alloy are presented in Table III. The corresponding diffusion coefficients are presented in Figure 23. As can be seen in the figure, the data obtained for Armco ingot iron lie in between the data reported by Gonzalez (ref. 31) and Nelson (ref. 39). The diffusion results are internally consistent and again clearly indicate that diffusivity decreases as the carbon content increases. As in the case of permeation, thermally activated Arrhenius behavior is indicated throughout the carbon composition range. The diffusion activation energy is dependent on the carbon content as shown in Table III although the pre-exponential constant remains constant

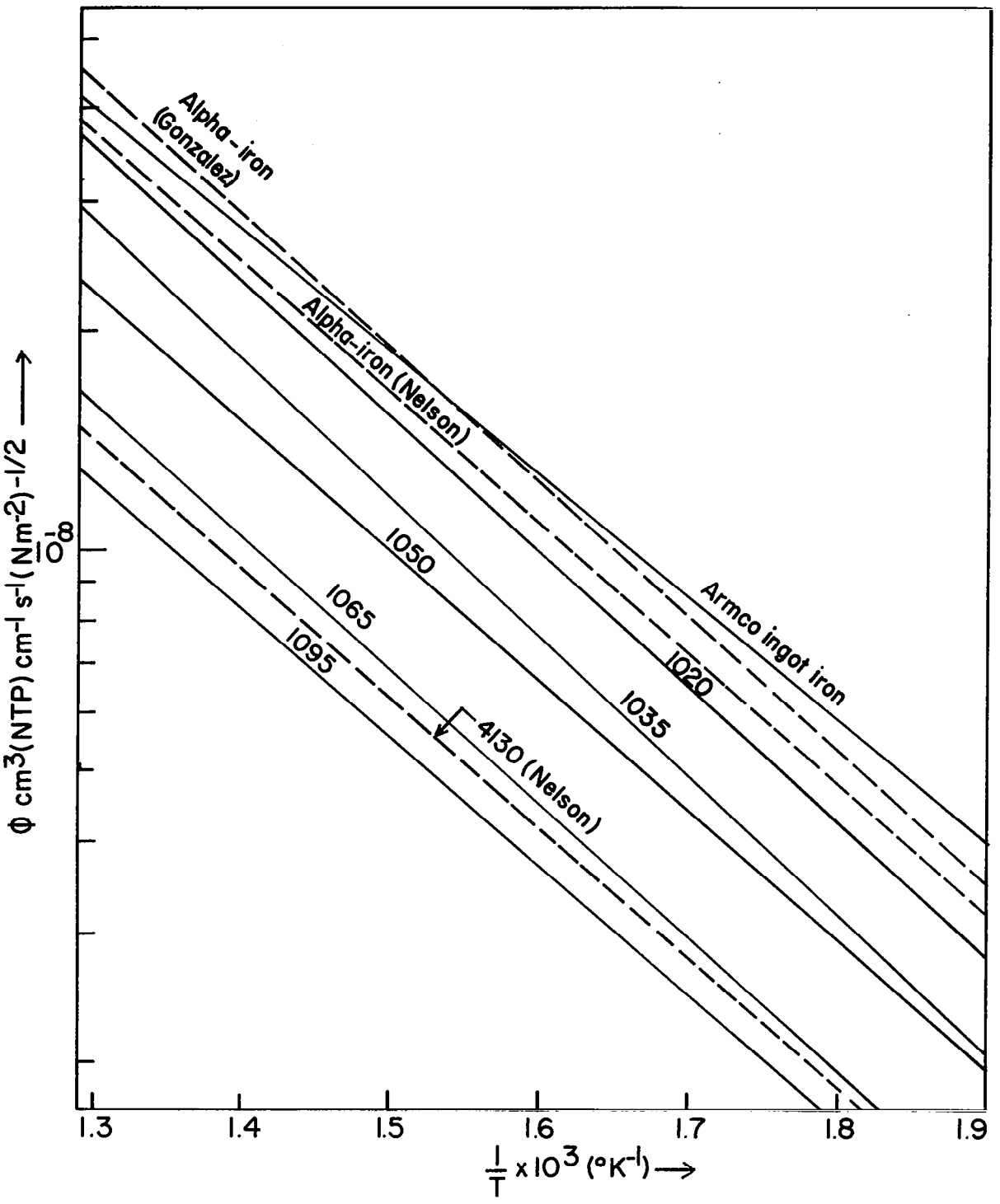

Figure 21. - The effect of carbon content on the coefficient of hydrogen permeation in normalized carbon steels as a function of temperature

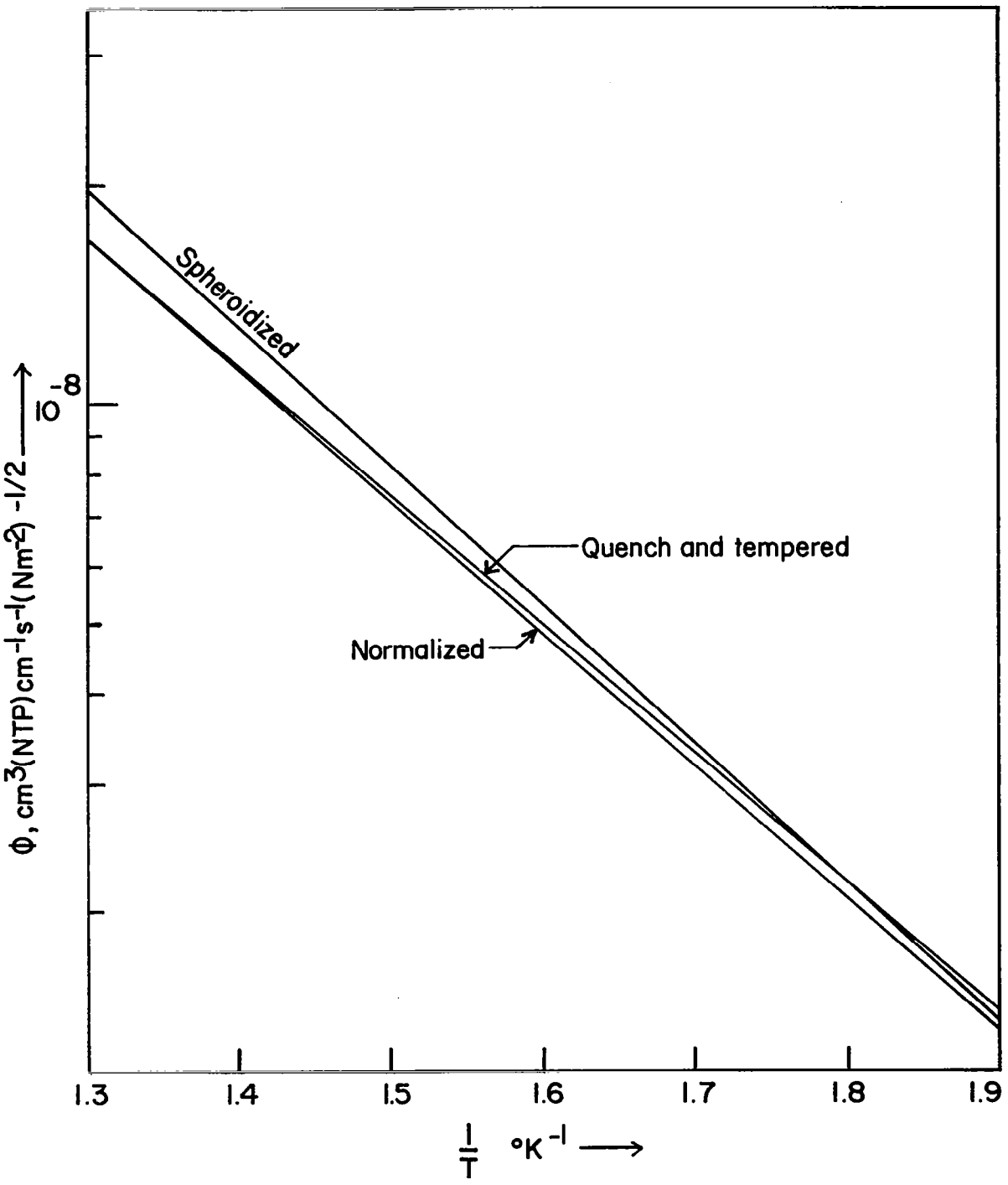

Figure 22. - The effect of heat treatment on the coefficient of hydrogen permeation in 1065 steel as a function of temperature

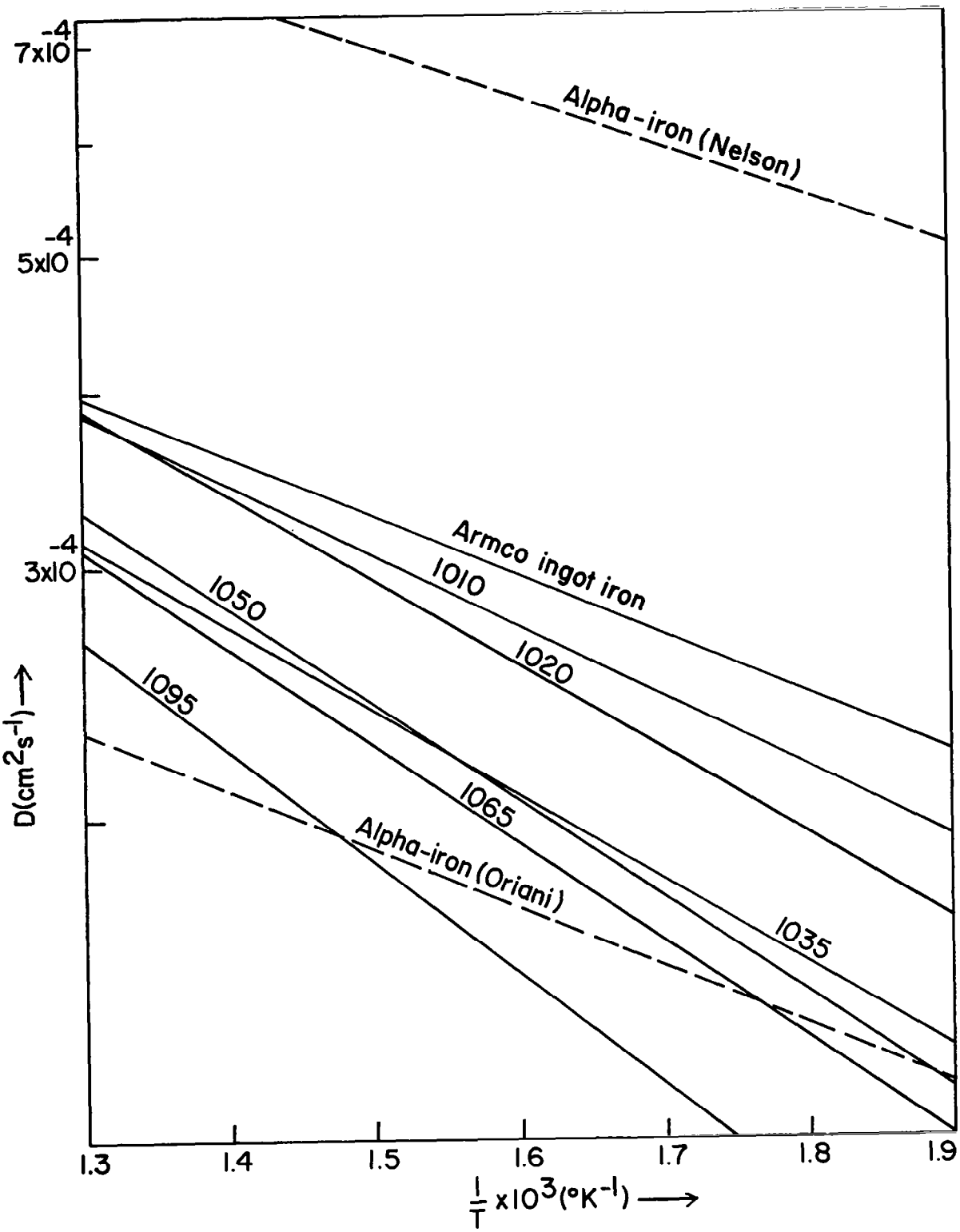

Figure 23. - The effect of carbon content on the coefficient of hydrogen diffusion in normalized carbon steels as a function of temperature

within experimental error. These dependencies are just opposite of what are observed for permeation.

TABLE III. - ARRHENIUS CONSTANTS FOR HYDROGEN DIFFUSIVITY IN ALPHA-IRON AND NORMALIZED CARBON STEELS

Alloy	$D_o \times 10^3$	Q_D
Armco Ingot Iron	1.395	8,030 ± 1650
SAE 1010	1.700	9,480
1020	2,370	11,530
1035	1.910	11,530
1050	2.530	13,030
1065	2.440	13,190
1095	2.475	14,150

Effect of Heat Treatment - The pre-exponential constant and diffusion activation energy for 1065 steel in the three heat treated conditions are presented in Table IV.

TABLE IV. - ARRHENIUS CONSTANTS FOR HYDROGEN DIFFUSIVITY IN 1065 STEEL AS A FUNCTION OF HEAT TREATMENT

Alloy Condition	$D_o \times 10^3$	Q_D
Quench and tempered	2.308	11,025 ± 1200
Spheroidized (in situ)	2.800	12,820
Normalized	2.350	13,490

The corresponding diffusion coefficients are presented in Figure 24. As can be seen in the figure, diffusivity is maximum in the quench and tempered structure and is minimum in the normalized fine pearlite structure. As commented on earlier, Robertson (ref. 41) obtained similar results. Thermally activated Arrhenius behavior is indicated for all heat treatments.

SOLUBILITY

Effect of Carbon Content - The solubility constants for hydrogen solution in each carbon steel alloy are presented in Table V. The corresponding solubilities are presented as a function of temperature at constant pressure in Figure 25. The results indicate that the solubility decreases as the carbon content increases. On first examination, this would seem to contradict a

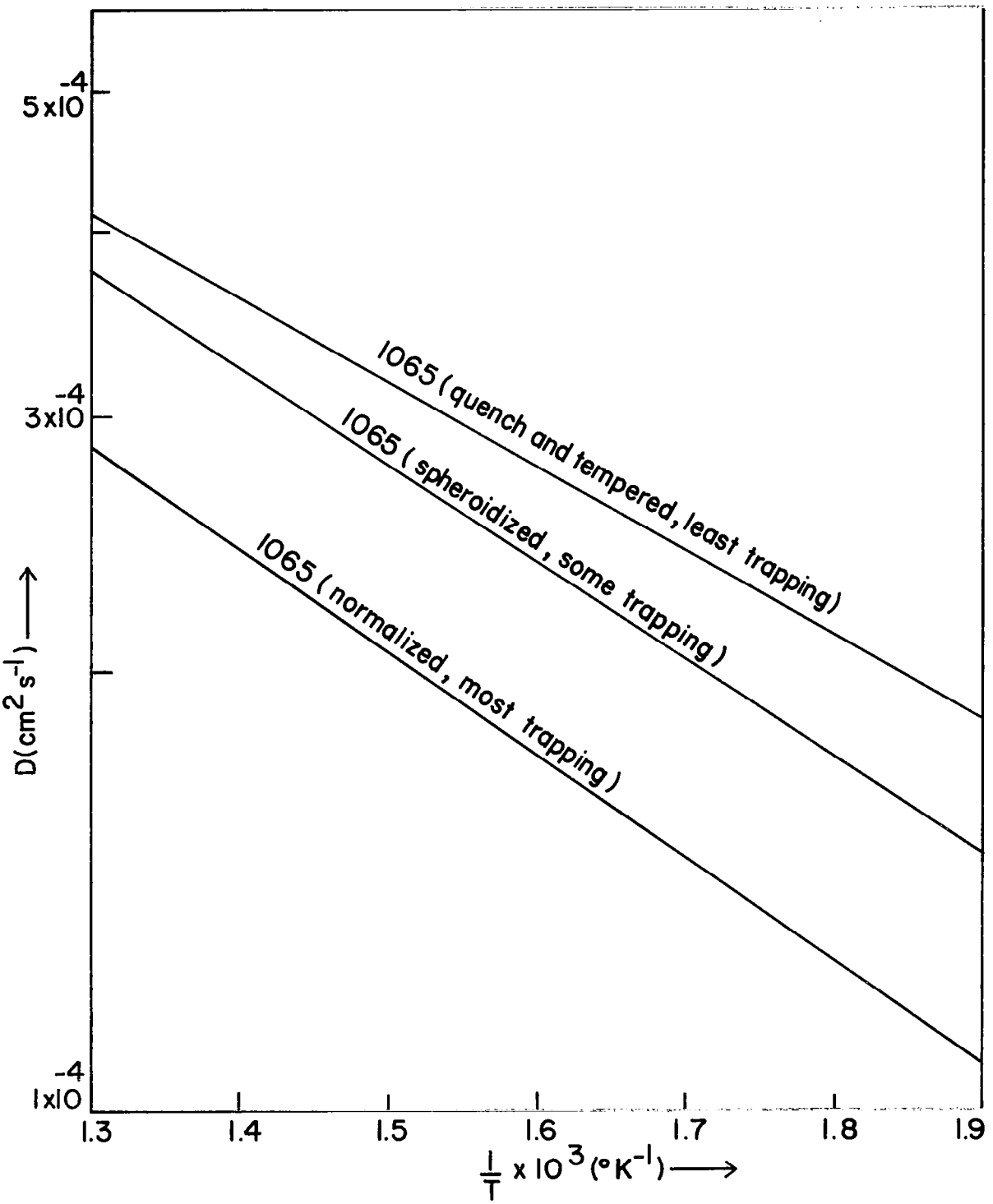

Figure 24. - The effect of heat treatment on the coefficient of hydrogen diffusion in 1065 steel as a function of temperature

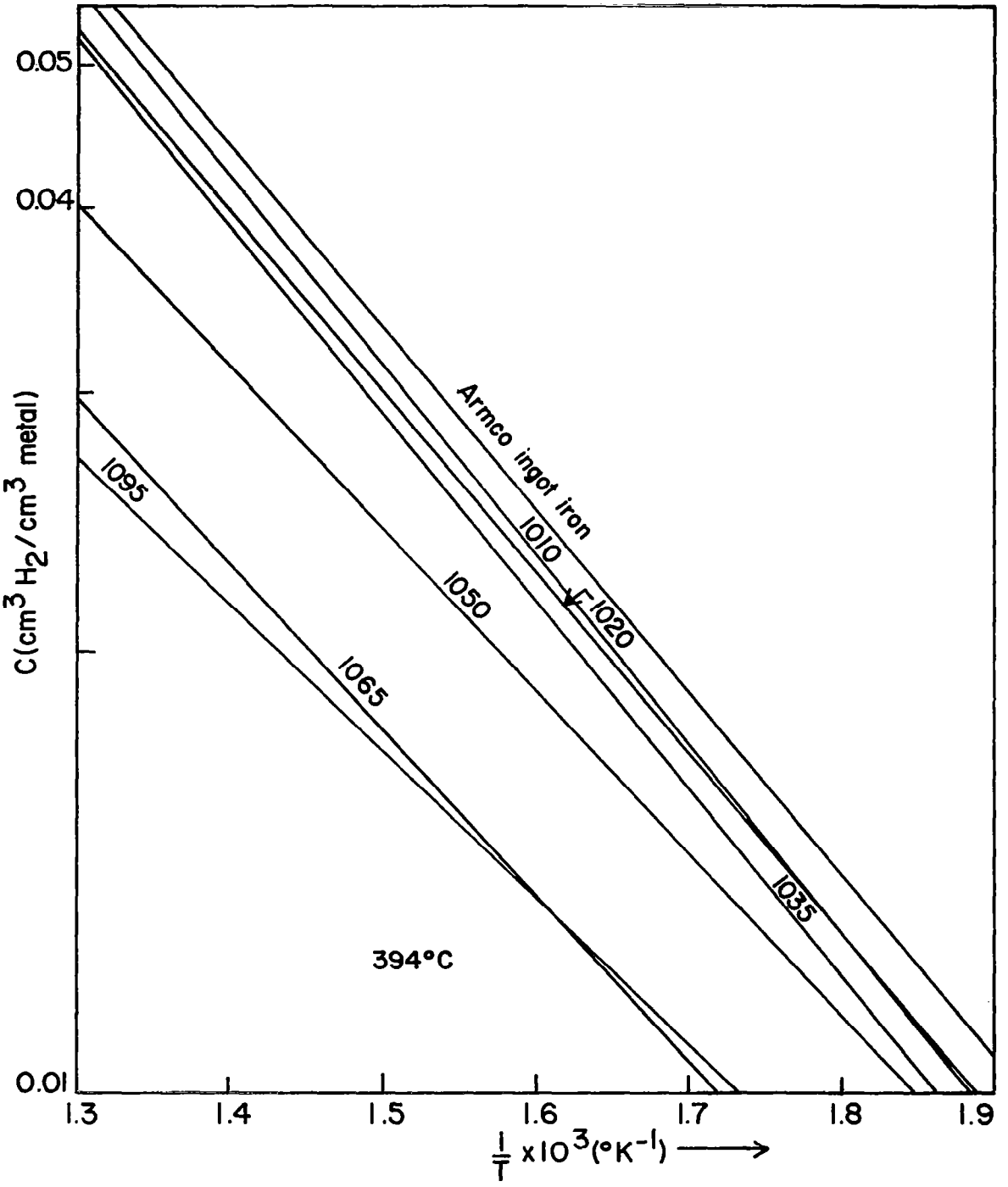

Figure 25. - The effect of carbon content on the solubility of hydrogen in normalized carbon steels as a function of temperature at 3.447 X 10^5 Nm^{-2} hydrogen pressure

trapping mechanism but, as will be discussed later, it is entirely consistent based on ferrite/carbide ratio.

TABLE V. - SOLUBILITY CONSTANTS FOR HYDROGEN SOLUTION IN ALPHA-IRON AND NORMALIZED CARBON STEELS

Alloy	$(\phi_o/D_o)\ p_a^{\frac{1}{2}}$	ΔH_s
Armco Ingot Iron	$4.038 \times 10^{-3}\ p_a^{\frac{1}{2}}$	-23,660
SAE 1010	$4.538 \times 10^{-3}\ p_a^{\frac{1}{2}}$	-24,700
1020	$3.565 \times 10^{-3}\ p_a^{\frac{1}{2}}$	-23,540
1035	$4.228 \times 10^{-3}\ p_a^{\frac{1}{2}}$	-24,630
1050	$1.858 \times 10^{-3}\ p_a^{\frac{1}{2}}$	-21,100
1065	$1.471 \times 10^{-3}\ p_a^{\frac{1}{2}}$	-21,540
1095	$0.941 \times 10^{-3}\ p_a^{\frac{1}{2}}$	-19,270

Effect of Heat Treatment - The solubility constants for hydrogen solution in 1065 steel in the quench and tempered, spheroidized, and normalized conditions are presented in Table VI. The corresponding solubilities are presented as a function of temperature at constant pressure in Figure 26. The normalized structure exhibits the highest solubility while the spheroidized and quench and tempered structure exhibit the lowest.

TABLE VI. - SOLUBILITY CONSTANTS FOR HYDROGEN SOLUTION IN 1065 STEEL AS A FUNCTION OF HEAT TREATMENT

Alloy Condition	$(\phi_o/D_o)\ p_a^{\frac{1}{2}}$	ΔH_s
Quench and tempered	$1.428 \times 10^{-3}\ p_a^{\frac{1}{2}}$	-22,775
Spheroidized (in situ)	$2.154 \times 10^{-3}\ p_a^{\frac{1}{2}}$	-23,740
Normalized (in situ)	$1.648 \times 10^{-3}\ p_a^{\frac{1}{2}}$	-21,270

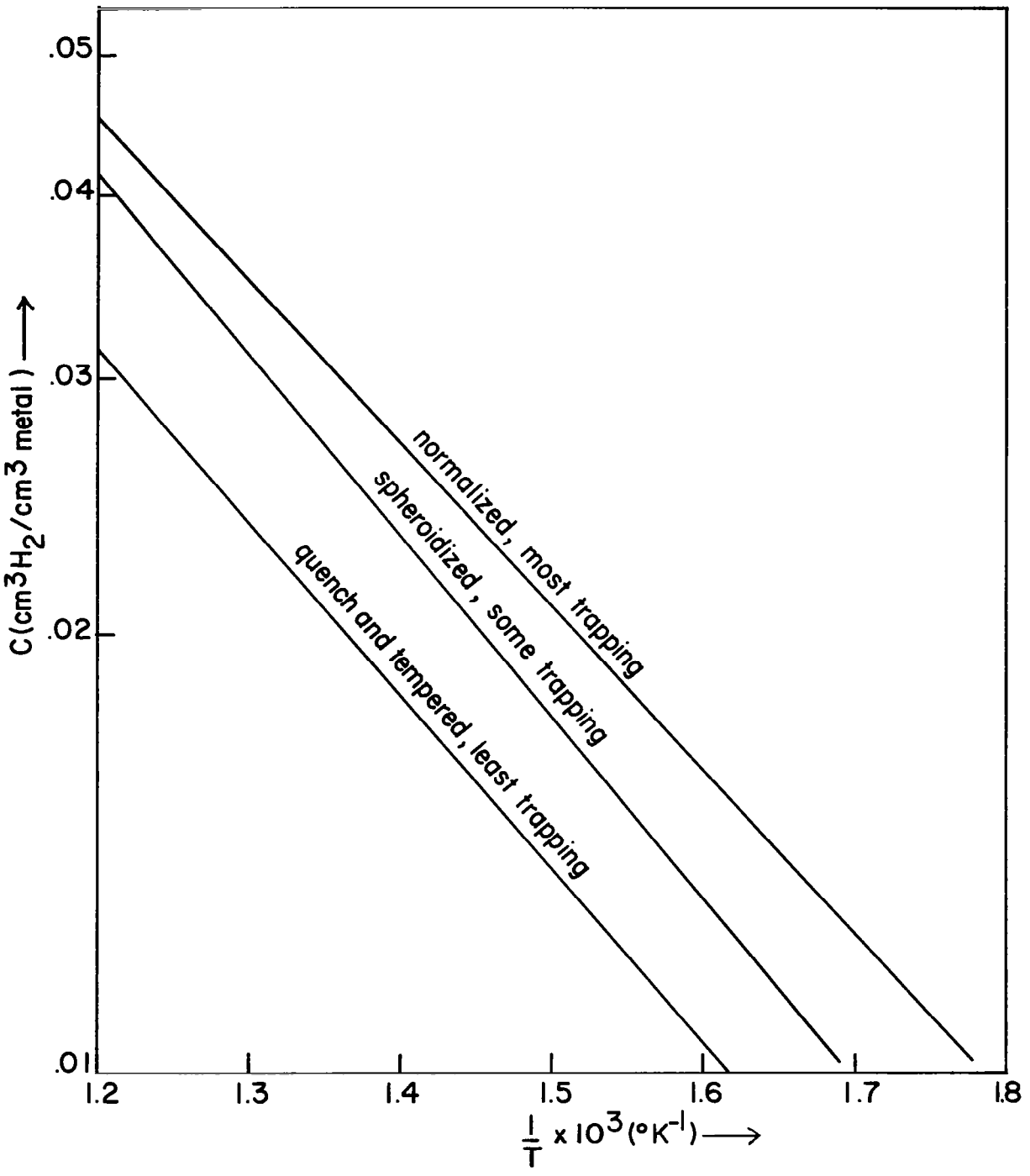

Figure 26. - The effect of heat treatment on the solubility of hydrogen in 1065 steel as a function of temperature at 3.447 X 10^5 Nm^{-2} hydrogen pressure

DISCUSSION

Oriani (ref. 44) suggested that trapping at solid-solid interfaces such as carbide-alpha iron is operative in the absence of cold work. As the carbon content increases, the interfacial area between carbide-alpha iron increases, more hydrogen is trapped and the diffusivity decreases as was observed in this investigation. Heat treatment had a substantial effect on the diffusivity since the carbide interfacial area was altered during heat treatment. Carbide associated with fine pearlite appears to promote maximum hydrogen trapping and minimum diffusivity whereas the quench and tempered structure exhibited minimum hydrogen trapping and maximum diffusivity. The spheroidized structure showed a somewhat higher diffusivity than the normalized structure because of the coalescence of carbide and the associated reduction of interfacial area. The results of the study on the effect of heat treatment are in good agreement with the observations of others (refs. 39,40,41) and confirm the suggestion that interfacial trapping is operative during unsteady state transport in carbon steels.

The decrease in the solubility with increase in carbon content does not appear to be consistent with a trapping model since the solubility would be expected to increase. However, further examination suggests an explanation based on the ratio of trapped to lattice hydrogen. Assuming that trapped hydrogen accumulates at ferrite-carbide interfaces in pearlite and that soluble hydrogen is absorbed in pro-eutectoid ferrite in the ratio of microconstituent masses, calculations show that the ratio of trapped to lattice hydrogen is about 0.085 in 1010 steel and increases to about 4.4 in 1065 steel. Obviously, the trapped hydrogen concentration is increasing as the amount of carbide increases although the actual result is a decrease in solubility because the amount of pro-eutectoid ferrite is decreasing. Hydrogen solubility data for 1065 steel after heat treatment is entirely consistent with a trapping model since the solubility and corresponding trapping was maximum in a normalized structure and minimum in a quench and tempered structure. No discontinuities were observed in the solubilities of any of the carbon steels computed from experimental data (ref. 45).

Hydrogen permeability is substantially reduced by second phase precipitates according to Levchenko et al. (ref. 46) and the reason that it is lower in higher carbon steels is probably related to the combined effect of an increase in the amount of carbide in higher carbon steels and the corresponding lower hydrogen permeability in the carbide phase (ref. 40). Additionally, the permeability is directly proportional to the diffusivity according to Sievert's Law so that one would expect both the permeability and diffusivity to decrease for transport processes controlled by lattice diffusion.

CONCLUSION

The following conclusions pertain to hydrogen gas-phase transport experiments conducted at temperatures between 250° and 600°C and pressures between 1.013×10^5 Nm^{-2} and 4.052×10^5 Nm^{-2}:

1) Lattice diffusion controls steady and unsteady state transport through normalized and heat treated carbon steels containing up to about 1.2 w/oC.
2) Permeability and diffusivity decrease in normalized carbon steels as the carbon content increases.
3) Permeability is independent of heat treatment whereas diffusivity is maximum in quench and tempered structure and minimum in normalized structure.
4) Diffusivity and solubility data are consistent with a trapping model involving solid-solid interfaces such as ferrite-iron carbide.
5) Based on lattice diffusion controlled transport and Sievert's Law, expressions for coefficient of hydrogen permeation, coefficient of hydrogen diffusion and solubility constants were obtained from experimentally determined steady state and lag-time measurements in normalized carbon steels as follows:

For Armco Ingot Iron
$\phi = 5.633 \times 10^{-6} \exp(-31{,}690/RT)$
$D = 1.395 \times 10^{-3} \exp(-8{,}030/RT)$
$C = 4.038 \times 10^{-3} p^{\frac{1}{2}} \exp(-23{,}660/RT)$

For 1010 steel
$\phi = 7.715 \times 10^{-6} \exp(-34{,}180/RT)$
$D = 1.700 \times 10^{-3} \exp(-9{,}480/RT)$
$C = 4.538 \times 10^{-3} p^{\frac{1}{2}} \exp(-24{,}700/RT)$

For 1020 steel
$\phi = 8.45 \times 10^{-6} \exp(-35{,}070/RT)$
$D = 2.370 \times 10^{-3} \exp(-11{,}530/RT)$
$C = 3.565 \times 10^{-3} p^{\frac{1}{2}} \exp(-23{,}540/RT)$

For 1035 steel
$\phi = 8.076 \times 10^{-6} \exp(-36{,}160/RT)$
$D = 1.910 \times 10^{-3} \exp(-11{,}530/RT)$
$C = 4.228 \times 10^{-3} p^{\frac{1}{2}} \exp(-24{,}630/RT)$

For 1050 steel
$\phi = 4.700 \times 10^{-6} \exp(-34{,}130/RT)$
$D = 2.530 \times 10^{-3} \exp(-13{,}030/RT)$
$C = 1.858 \times 10^{-3} p^{\frac{1}{2}} \exp(-21{,}100/RT)$

For 1065 steel
$\phi = 3.590 \times 10^{-6} \exp(-34{,}730/RT)$
$D = 2.440 \times 10^{-3} \exp(-13{,}190/RT)$
$C = 1.471 \times 10^{-3} p^{\frac{1}{2}} \exp(-21{,}540/RT)$

For 1095 steel
$\phi = 2.328 \times 10^{-6} \exp(-33{,}420/RT)$
$D = 2.475 \times 10^{-3} \exp(-14{,}150/RT)$
$C = 0.941 \times 10^{-3} p^{\frac{1}{2}} \exp(-19{,}270/RT)$

REFERENCES

1. Shah, K. K.: Gas-Phase Hydrogen Transport in Titanium. Ph.D. Thesis, University of Nebraska, May 1975.

2. Reeves, B. L.: Geometry Effects on the Transport of Hydrogen in α-Phase Titanium. M.S. Thesis, University of Nebraska, May 1976.

3. Johnson, D. L.; and Nelson, H. G.: Determination of Hydrogen Permeation Parameters in Alpha Titanium Using the Mass Spectrometer. Met. Trans. Vol. 4, Feb. 1973, pp. 569-573.

4. Lenning, G. A.; Craighead, C. M.; and Jaffee, R. I.: Constitution and Mechanical Properties of Titanium-Hydrogen Alloys. Journal of Metals, Vol. 6, No. 3, Mar. 1954, pp. 367-376.

5. Williams, D. N.: Hydrogen in Titanium and Titanium Alloys. TML Report No. 100, Battelle Memorial Institute, May 16, 1958, pp. 1-110.

6. Gibb, T. R. P., Jr.; and Kruschwitz, H. W., Jr.: The Titanium-Hydrogen System and Titanium Hydride. Amer. Chem. Soc., Vol. 72, 1950, pp. 5365-5369.

7. Berger, L. W.; Williams, D. N.; and Jaffee, R. I.: Hydrogen in Titanium-Aluminum Alloys. Transactions AIME, Vol. 212, No. 4, Aug. 1958, pp. 509-513.

8. Schoenfelder, C. W.; and Swisher, J. H.: Kinetics of Thermal Decomposition of TiH_2. J. Vac. Sci. Technol., Vol. 12, No. 5, Sep.-Oct. 1973, pp. 862-870.

9. Shah, K. K.; and Johnson, D. L.: Effect of Surface Pre-oxidation on Hydrogen Permeation in Alpha Titanium. Proceedings of the Conference, Hydrogen in Metals, Vol. 2, American Society for Metals, Mar. 1974, pp. 475-481.

10. Wasilewski, R. J.; and Kehl, G. L.: Diffusion of Hydrogen in Titanium. Metallurgia, Vol. 50, No. 301, Nov. 1954, pp. 225-230.

11. Papazoglou, T. P.; and Hepworth, M. T.: The Diffusion of Hydrogen in Titanium. Trans. AIME, Vol. 242, No. 4, Apr. 1968, pp. 682-685.

12. McQuillan, A. D.: An Experimental and Thermodynamic Investigation of the Hydrogen-Titanium System. Proc. Roy. Soc. (London), Vol. 204, 1950, pp. 309-323.

13. Giorgi, T. A.; and Ricca, F.: Thermodynamic Properties of Hydrogen and Deuterium in α-Titanium. Suppl. al Nuovo Cinento, Vol. V, 1967, pp. 472-482.

14. Jackson, J. D.: Permeability of Titanium to Hydrogen. DMIC Tech Note, Battelle Memorial Institute, Columbus, Ohio, July 29, 1964, pp. 1-4.

15. Wickstrom, W. A.; and Etheridge, B. R.: Investigation into the Compatibility of Hydrogen and Titanium, Adv. in Cryogenic Eng., Vol. 13, 1968, pp. 334-342.

16. Caskey, G. R., Jr.: The Influence of a Surface Oxide Film on Hydriding of Titanium. Proceedings of the Conference on Hydrogen in Metals, ASM, Mar. 1974, pp. 465-474.

17. Reichardt, J. W.: The Kinetics of the Hydrogen-Titanium Reaction. J. Vac. Sci. Tech., Vol. 9, 1972, p. 548.

18. Williams, D. N.; and Maykuth, D. J.: Reaction of Titanium with Gaseous Hydrogen at Ambient Temperatures. Battelle Memorial Institute, DMIC Technical Note, Feb. 4, 1966.

19. Shah, K. K.; Nelson, H. G.; Johnson, D. L.; and Hamaker, F. M.: A Generalized Expression for Lag-Time in the Gas-Phase Permeation of Hollow Tubes. Met. Trans. A., Vol. 6A, Feb. 1975, pp. 373-375.

20. Phillips, J. R.; and Dodge, B. F.: Concentration-Dependent Time-Lag Measurements. A.I.Ch.E Journal, Vol. 14, No. 3, May 1968, pp. 392-397.

21. Frauenfelder, R.: Permeation of Hydrogen through Tungsten and Molybdenum. The Journal of Chemical Physics, Vol. 48, No. 9, May 1968, pp. 3955-3965.

22. Barrer, R. M.: Gas Flow in Solids. Phil. Mag., Vol. 28, July-Dec. 1939, pp. 148-162.

23. Barrer, R. M.: Diffusion in and through Solids. Cambridge Press, Cambridge, 1941, pp. 1-52.

24. Dushman, S.: Scientific Foundations of Vacuum Technology. Wiley and Sons, 1962, p. 80.

25. Johnson, D. L.; Bashara, N. M.; and Tao, L. C.: Oxide Film Growth on Titanium-Aluminum Alloys at 165-270°C. Materials Scienceand Engineering, Vol. 8, 1971, pp. 175-180.

26. Gulbransen, E. A.; and Andrew, K. F.: Kinetics of the Reactions of Titanium with O_2, N_2 and H_2. Jr. of Metals (Sec. 3) Trans., Vol. 1, No. 10, Oct. 1949, pp. 741-748.

27. Wang, J. Y. N.: Titanium and Titanium Alloys in Mercury--Some Observations on Corrosion and Inhibition. Nuclear Science and Engineering, Vol. 18, 1964, pp. 18-30.

28. Hauffe, K.: Oxidation of Metals. New York Plenum Press, 1965, pp. 7, 109-137, 209-228.

29. Quick, N. R.: The Relationship Between Concentration-Dependent Diffusion and Trapping in the Hydrogen-Iron System. M. S. Thesis, Cornell University, Jan. 1974.

30. Kumnick, A. J.; and Johnson, H. H.: Hydrogen Transport Through Annealed and Deformed Armco Iron, Met. Trans., Vol. 5, May 1974, pp. 1199-1206.

31. Gonzalez, O.D.: The Measurement of Hydrogen Permeation in Alpha Iron: An Analysis of Experiments. Met. Soc. of AIME Trans., Vol. 245, No. 4, Apr. 1969, pp. 607-612.

32. Choi, J. Y.: Diffusion of Hydrogen in Iron. Met. Trans., Vol. 1, Apr. 1970, pp. 911-919.

33. Oriani, R. A.: Hydrogen in Metals. Proc. Int. Conf., Fundamental Aspects of Stress Corrosion Cracking, Sept. 11-15, 1967, Ohio State Univ., Columbus. NACE, Houston, Texas, 1969, pp. 32-50.

34. Smialowski, M.: Hydrogen in Steel. Pergamon Press, Oxford, pp. 64-117, 35, 1962.

35. Eschbach, H. L.; Gross, F.; and Schulien, S.: Permeability Measurements with Gaseous Hydrogen for Various Steels. Vacuum, Vol. 13, 1963, pp. 543-547.

36. Fletcher, E. E.; and Elsea, A. R.: Hydrogen Movement in Steel--Entry, Diffusion and Elimination. DMIC-219, Battelle Memorial Institute, Columbus, Ohio, p. 50, June 30, 1965.

37. Mindyuk, A. K.; and Svist, E. I.: The Diffusion Mobility of Hydrogen in Iron and Steel Allowing for Phase Transformations. Plenum Publishing Corp.,New York, 1975, pp. 34-38.

38. Angeles, O. F.; Stueber, R. J.; and Geiger, G. H.: Hydrogen Diffusion Coefficients in Ferrovac 1020 and Cr-Mo Alloy Steels. Corrosion, Vol. 32, No. 5, May 1976, pp. 179-183.

39. Nelson, H. G.; and Stein, J. E.: Gas-Phase Hydrogen Permeation through Alpha Iron, 4130 Steel and 304 Stainless Steel from Less than 100°C to Near 600"C. NASA TN D-7265, Apr. 1973, pp. 1-18.

40. Nikonorova, A. I.; Borisova, N. S.; Ammosova, L. M.; and Shiryaev, A. G.: Effect of Heat Treatment on Hydrogen Permeability of Structural Steels. Plenum Publishing Corp., New York, NY, June 1972, pp. 339-341.

41. Robertson, W. M.: Hydrogen Permeation and Diffusion in 1045 Steel in Different Heat Treated Conditions. TMS-AIME Fall Meeting Abstracts, Oct. 24-27, 1977, p. 31.

42. Kikuya, Y.; and Araki, T.: A Fundamental Research on the Diffusivity of Hydrogen in Steel, and Its Effect on the Embrittlement and Delayed Failure of Steel. Proceedings of the Symposium on Precaution of Cracking in Welded Structures based on Recent Theoretical and Practical Knowledge, Japan Weld. Soc., Tokyo, Japan, 1972, pp. II B 3.1-II B 3.12.

43. Yoshizawa, S.; and Yamakawa, K.: Studies on Permeation Rate of Hydrogen Through Cold Worked Iron. Proceedings of the International Conference on Metallic Corrosion, Natl. Assoc. of Corrosion Engr., NACE-3, 1974, pp. 421-427.

44. Oriani, R. A.: The Diffusion and Trapping of Hydrogen in Steel. Acta Metallurgica, Vol. 18, Jan. 1970, pp. 147-157.

45. Weizer, V. G.: Behavior of Hydrogen in α-Iron at Lower Temperatures. NASA TN D-7514, Dec. 1973.

46. Levchenko, V. P.; Gol'tsov, V. A.; and Gel'd, P. V.: Hydrogen Permeability of Annealed and Deformed Carbon Steels with Lamellar Pearlite Structure. Soviet Materials Science, Vol. 5, No. 2, 1969, pp. 138-141.